Applied Surface Science

Influence of fractal and lacunar characteristic of a nanostructured substrate on SERS enhancement

--Manuscript Draft--

Manuscript Number:	APSUSC-D-20-07138R1
Article Type:	Full Length Article
Keywords:	SERS, silicon nanowires, fractal nanostructure, lacunarity, SERS substrate
Corresponding Author:	Dubravko Risovic, Ph.D. Rudjer Boskovic Institute Zagreb, CROATIA
First Author:	Dubravko Risovic, Ph.D.
Order of Authors:	Dubravko Risovic, Ph.D.
	Hrvoje Gebavi, PhD.
	Mile Ivanda, PhD
Abstract:	Nanostructured materials play a significant role in numerous advanced and diversified applications many of which exploit their optical properties. Among these are nanostructured substrates for Surface-enhanced Raman scattering (SERS). The objective of our study was to contribute to understanding of topological aspects influencing and underlying SERS on nanostructured substrates. To that purpose we fabricated Ag-decorated Si-nanowires (SiNWs) substrates with different fractal and lacunar characteristics. We demonstrated that fractal dimension and lacunarity have a profound influence on SERS enhancement. We discussed the involved interplay between long-range properties of nanostructured substrate, namely its fractal topology, and short-range local features on a nanometer scale related to the distribution of inter-wire gaps (i.e. lacunarity) which strongly affect the local field enhancement, altogether precipitating in significant increase of SERS. Explanation of a strong correlation found to exist between fractal dimension D , lacunarity and SERS enhancement and the observed abrupt increase of SERS at D » 2.54 are provided within the framework of the percolation theory. For a percolated fractal structure a strong enhancement depends on the excitation wavelength resonantly matching the heterogeneity sizes of inter nanowire gaps as characterized with a high lacunarity determining the distribution of localized optical excitations i.e. hot spots.

APPLIED SURFACE SCIENCE
Dr. Tadahiro Komeda, Editor

Zagreb, July 30. 2020.

Dear Dr. Komeda,

Please find attached the revised manuscript (APSUSC-D-20-07138) entitled "***Influence of fractal and lacunar characteristic of a nanostructured substrate on SERS enhancement***" by D. Risović*, H. Gebavi* and M. Ivanda.

In the revision we have addressed all issues/questions raised by the reviewer and to that purpose included new paragraphs, a new Appendix and new pertinent references as well as some new results/data. In our opinion this resulted in an improved manuscript compliant with reviewer's recommendations.

In the revision the changes are denoted in blue.

Sincerely,

Dr.sc. Dubravko Risović

HIGHLIGHTS

- Topological features, particularly lacunarity and fractal dimension determine characteristics of nanostructured materials

- Fractal dimension and lacunarity of a nanostructured substrate have a profound influence on SERS

- Percolation results in abrupt increase of SERS enhancement

- Fractal and lacunar characteristics of a substrate are determined with fabrication temperature

GRAPHICAL ABSTRACT

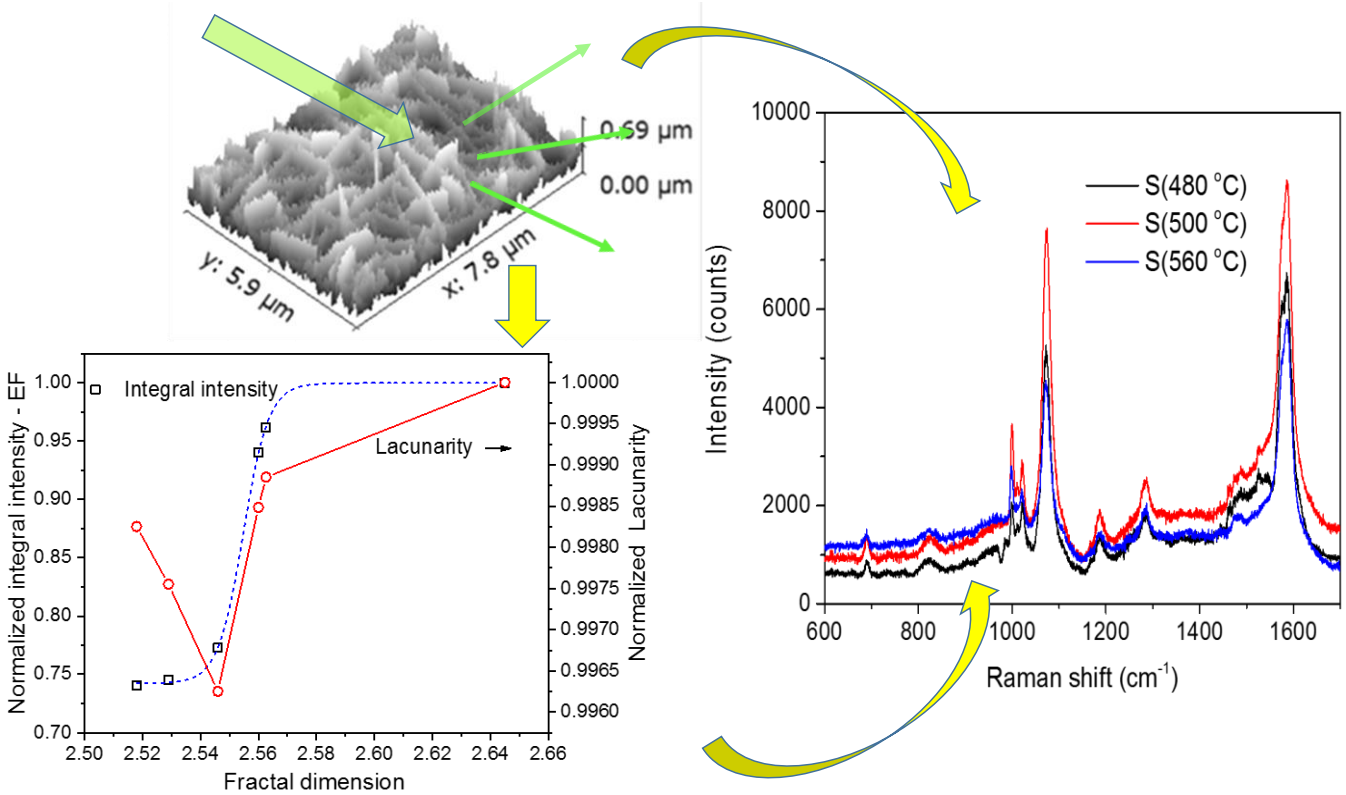

Influence of fractal and lacunar characteristic of a nanostructured substrate on SERS enhancement

Dubravko Risović*[1], Hrvoje Gebavi*[1] and Mile Ivanda[1]

[1] Ruđer Bošković Institute, Division of Materials Physics, Laboratory for Molecular Physics and Synthesis of New Materials, and Centre of Excellence for Advanced Materials and Sensing Devices, Research Unit New Functional Materials, Bijenička c. 54, HR-10000 Zagreb, Croatia

ABSTRACT

Nanostructured materials play a significant role in numerous advanced and diversified applications many of which exploit their optical properties. Among these are nanostructured substrates for surface-enhanced Raman scattering (SERS). The objective of our study was to contribute to understanding of topological aspects influencing and underlying SERS on nanostructured substrates. To that purpose we fabricated Ag-decorated Si-nanowires (SiNWs) substrates with different fractal and lacunar characteristics. We demonstrated that fractal dimension and lacunarity have a profound influence on SERS enhancement. We discussed the involved interplay between long-range properties of nanostructured substrate, namely its fractal topology, and short-range local features on a nanometer scale related to the distribution of inter-wire gaps (i.e. lacunarity) which strongly affect the local field enhancement, altogether precipitating in significant increase of SERS. Explanation of a strong correlation found to exist between fractal dimension D, lacunarity and SERS enhancement and the observed abrupt increase of SERS at $D \approx 2.54$ are provided within the framework of the percolation theory. For a percolated fractal structure a strong enhancement depends on the excitation wavelength resonantly matching the heterogeneity sizes of inter nanowire gaps as characterized with a high lacunarity determining the distribution of localized optical excitations i.e. hot spots.

Keywords: *SERS, silicon nanowires, fractal nanostructure, lacunarity, SERS substrate,*

Introduction

Generally, optical properties of nanostructured materials play paramount role in numerous advanced and diversified applications. Among these is use of nanostructured substrates for Surface-Enhanced Raman Scattering (SERS) whose optical properties have profound influence on enhancement of Raman signal. SERS is a highly sensitive spectroscopic technique exploiting the effect of enhancement of weak Raman scattering by molecules adsorbed on nanostructured or rough metal surfaces. The exact mechanism of the enhancement effect of SERS is still a matter of debate in the literature. However, it is now generally agreed that the dominant contributor to SERS processes is the electromagnetic enhancement mechanism [1]. According to this model the inherently weak Raman signals, originating from molecules adsorbed on a substrate's surface are enhanced by several orders of magnitude if the molecules are localized in nanoscale regions of intense optical fields i.e. trapped between adjacent plasmonic surfaces in the substrate, so-called "hot-spots" [2]. Since the SERS signal intensity depends on analyte - plasmon interaction occurring after adsorption of the analyte molecules onto the SERS substrate, the SERS substrate plays a paramount role in the enhancement process. In that context, among the great variety of SERS substrates [3] the attention has recently turned towards fractal nanostructures due to their exceptional performances in SERS. Theoretically, such structures cannot support ordinary wave propagation due to their lack of translational invariance. Hence, plasmonic waves become localized within fractals. Since the long-range interactions are suppressed, the individual dipolar modes of metallic particles, being spatially localized, enhance the field within these nanoscopic substrate regions resulting in exceptional SERS enhancement [4, 5].

Recently, the use of silicon nanostructures, particularly silicon nanowires (SiNWs) as SERS substrates draw considerable attention [6-9]. This interest is motivated by high enhancement factors, large surface-to-volume ratios, high measurement reproducibility and relatively low-cost fabrication compatible with the well-established silicon technology. In regard to investigations of SiNWs structures, these were mostly limited to 2d arrays of vertically oriented wires, while less attention has been devoted to the investigation of random 3d structures [10-17].

As far as our knowledge goes so far there was no systematic inquiry into the relationship between characteristics of random fractal structures, namely values of fractal dimension and lacunarity, and its optical properties, particularly the enhancement of Raman scattering.

Furthermore, it is well known that percolation, a second order phase transition often results in dramatic changes in structure's properties. Hence, we expect that percolation occurring in nanostructures such as random silicon nanowires structure should have a profound influence on its optical properties, particularly regarding SERS, since the theory predicts that "hot spots" are much stronger at percolation thresholds [18]**.** However, so far this aspect has not been given sufficient attention.

In this context, our aim was to investigate the relation between fractal substrate structure, characterized by its fractal dimension and lacunarity, and Raman light scattering enhancement in relation to percolation. To that purpose we have used a substrate consisting of 3d randomly oriented SiNWs decorated with silver nanoparticles.

We demonstrate that on the one hand the strong Raman enhancement is strictly correlated with the substrate's fractal dimension, which in turn can be controlled with the synthesis temperature and, on the other hand, length scales at which the refractive index primarily fluctuates governed by structure's lacunarity. The observed results are explained within the framework of the percolation theory. Particularly we show that the abrupt change in SERS is result of a second order phase transition - percolation occurring in the nanostructure.

1. Methods

2.1. Nanowire synthesis and substrate fabrication

We synthetized samples of randomly oriented SiNWs intended to be used as SERS substrates on p-type Si substrates (⟨100⟩ orientation, and 5–10 Ωcm resistivity) by a vapour – liquid – solid (VLS) growth method in a low – pressure chemical vapour deposition (LPCVD) reactor using previously reported method [9]. Briefly, we first cleaned Si wafers applying standard cleaning procedures [19] followed by the thin pre-layer Au sputtering in Polaron E5000 sputter coater. Next, prior to application of the VLS method, we performed annealing for one hour at temperatures from 480°-560°C. The VLS process was carried out with 26% SiH_4 diluted in Ar at 270 sccm flow rate during 1h deposition period. In each experiment, the annealing temperature was the same as VLS deposition temperature. We decorated the randomly orientated

SiNWs obtained in the previous step by Ag nanoparticles using the same sputtering system for several minutes under constant Ar flow.

2.2. SERS measurements

For SERS measurements, the 3x3 mm size substrate samples were immersed in ethanol solution of mercaptophenylboronic acid $C_6H_7BO_2S$ (4-MPBA) for several hours and subsequently dried.

The Raman spectroscopy measurements were performed on Jobin Yvon T64000 Raman spectrometer in micro-single configuration. The laser power at 532 nm on the sample with ~1μm spot size was ~1–2 mW. For all experiments, the 50x/0.75 objective was used. Exposition time was 20s for 1 scan. Mapping features: 100 points, 10 μm step, 1 scan/point, 10 s/sc.

2.3 Fractal analysis

Fractal and lacunarity analysis were performed on grey-scale SEM images using Fractal 3e [20], Frac-Lac, a plug-in for Image J [21] and Gwyddion [22] software.

There are several methods available for determination of fractal dimension [23] from the grey-scale images (pixel intensity values 0-255) which are used by different software. Our selection of the method for determination of fractal dimension was based on its appropriateness for the problem at hand and on comparative evaluation of performances, advantages and disadvantages of various methods, as discussed in the literatule [23, 24].

We used Fractal 3e software [20] that uses the Difference statistics (dynamic scaling) method [25]. The *Difference Statistics (Dynamic Scaling) method* suitable for grey scale images, relies on establishing the difference function $\Delta f(\varepsilon)$ as a function of spatial scale, as described in Refs. [23] and [25]:

$$\Delta f(\varepsilon) = \langle [f(x,y) - f(x_0,y_0]^2 \rangle^{1/2} \quad (1)$$

Here, $f(x_0,y_0)$ is the value of the considered function (representing height or intensity) at reference point and $f(x, y)$ is its value at a point at distance ε from the reference point. The

difference is averaged over spatial extent of the considered surface/image. If the considered function is the height *h* then the difference function $\Delta h(\varepsilon)$ is also known as *hight-hight* correlation function.

Now, for $\varepsilon \leq \xi$:

$$\Delta f(\varepsilon) \sim \varepsilon^{H} \tag{2}$$

Here, ξ is lateral correlation length and $H = d\text{-}D$ is Hurst or Hölder exponent related to the embedding and fractal dimensions *d* and *D*, respectively [26-29].

Hence, taking the logarithm of both sides of Eq. 2 and letting ε to go to zero, the fractal dimension (in a three dimensional space) is obtained as [28]:

$$D = \lim_{\varepsilon \to 0} \left[3 - \frac{\log \Delta f(\varepsilon)}{\log \varepsilon} \right] \tag{3}$$

2.4. Lacunarity analysis

Lacunarity is generally inferred from patterns extracted from digital images using box counting method. The arrangement of pixels is examined using box-shaped elements from a set of arbitrary sizes, denoted ε. The box of size ε is placed successively over the entire image, and the number of pixels that fall within the box is recorded. Thus, from the pixel distribution in an image, obtained from scans at different box sizes and at different grid orientations (g) the lacunarity $\lambda(\varepsilon, g)$ is calculated as

$$\lambda(\varepsilon,g) = CV(\varepsilon,g)^2 = (\sigma/\mu)^2_{\varepsilon,g} \tag{4}$$

where *CV* is the coefficient of variation, σ and μ are standard deviation and mean for pixels per box at size ε, and orientation g [30,31]. Hence, there is a value of λ for each ε from each series of grid sizes and for each g, from a set of grid orientations.

The result is usually presented as a plot of Ln (λ) *vs*. Ln (ε).To avoid the computationally awkward situations that may occur with homogenous images with vanishing standard deviations and consequently undefined slopes of regression lines the results are transformed to

$$\Omega\lambda = \lambda + 1 = (\sigma/\mu)^2 + 1 \quad (5)$$

The slope of ln-ln regression line of λ over all ε is calculated for each *g* using this equation to avoid an "undefined" calculation. Namely, a completely homogeneous image will not vary in the pixels per box, so that the standard deviation, σ, for a box count at some ε will be 0. This means that $\lambda = (\sigma/\mu)^2 = 0$, which makes sense, but it also means that the ln of λ and therefore the slope of the ln-ln regression line for λ and ε would be undefined. Thus, we transform the data using λ+1, so that a completely homogeneous image has a slope of 0, corresponding intuitively to the idea of no rotational or translational invariance and no gaps [21].

2. Results and Discussion

3.1. Fabrication and characterization of the fractal SiNWs substrates

Fabrication of the nanostructured SiNWs SERS substrate requires synthesis of SiNWs mesh and decoration of nanowires with Ag nanoparticles as described in the Methods. We synthetized randomly oriented SiNWs substrates at different temperatures in the range 480°C - 560°C, resulting in different substrate structures. The structures of the SiNWs substrates were examined using Jeol JSM 7000F scanning electron microscope (SEM) under 10 kV. For further characterization of the substrates we performed fractal and lacunar analysis of grey scale SEM images. Representative SEM images of SiNWs substrates (recorded at the same magnification), as well as their three-dimensional views, generated by the Gwyddion software, are depicted in Fig. 1. SEM images reordered at an order of magnitude higher magnification reveal the SiNW coverage with Ag nanoparticles. After short sputtering times (3 and 5 min), the SiNWs are relatively uniformly decorated with oval Ag nanoparticles of 20–40 nm diameter (Fig. A.1 in the Appendices).

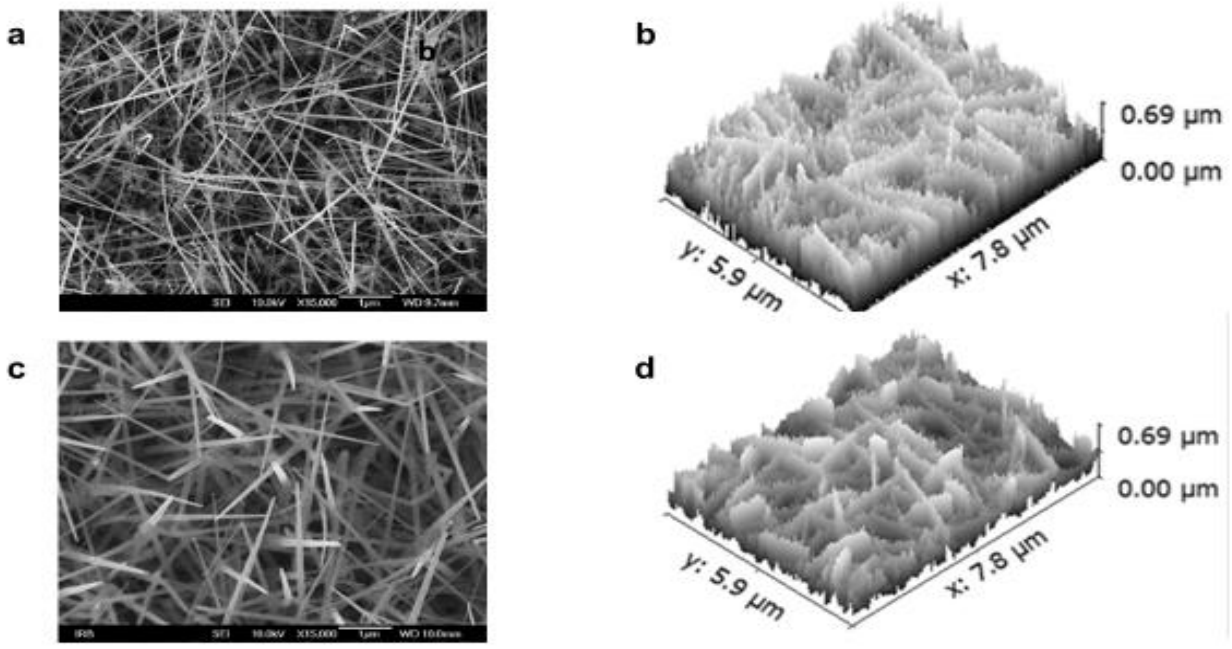

Fig. 1. SEM images and three dimensional views, of randomly oriented Si-nanowires SERS substrates. Substrates synthetized at T = 500 °C and at T = 560 °C are depicted in the upper (a-b) and lower (c-d) rows, respectively. The recorded SEM images (magnification 15000x), with dimensions 1280x1024 px, correspond to actual dimensions of 7.84 µm x 6.28 µm and height ≈ 0.7 µm (1px = 6.13nm).

In the SEM images similar yet distinctively different structures of SiNW substrates are clearly seen. The self - similarity of the substrate structures is revealed by inspecting SEM images taken at different magnifications (not shown here) and confirmed with subsequent fractal analysis. Analysis of the SEM images shows that the processing/synthesis temperature has a profound influence on structure and characteristics of substrates of randomly oriented SiNWs mesh. It also influences dimensions of the nanowires, particularly the thickness that increases with the increase of temperature viz. 45 – 70 nm and 120-180 nm for 500 ^{0}C and 560 ^{0}C, respectively. The surface roughness parameters inferred from SEM images (not presented here) also vary considerably and are correlated with the synthesis temperature as well as with the fractal dimension. The latter in compliance with the previous finding that there exists a strong correlation between certain roughness parameters and corresponding fractal dimension [32].

Next, we performed fractal and lacunarity analysis of grey scale SEM images. Fractal dimension D, as a measure of geometric complexity, is suitable for quantitative assessment of structures that are difficult to describe using classical Euclidean measures, and whose morphology is represented in binary or grayscale digital images. On the other hand, lacunarity can quantify additional features of patterns such as translational or rotational invariance and more generally, heterogeneity of a fractal structure. Lacunarity, being a measure of spatial heterogeneity provides means that can distinguish between two objects that have the same D but are structurally different. Thus, it can be used to differentiate between SEM images that have similar fractal dimensions but different appearances.

Firstly, we performed fractal analysis as described in the Methods. The analysis of SEM images established the fractal character of all considered substrates as documented further on.

Values of fractal dimensions D_g of SiNWs substrates inferred from their grey-scale SEM images are depicted in Fig. 2. D_g (subscript "*g*" denotes that the fractal dimension was derived from grey scale images) corresponds to the volume structure of the substrate, hence $2 < D_g < 3$. A higher value of D_g indicates that the considered fractal structure has a higher space-filling capacity. Obviously, all considered SiNWs substrates are fractal structures yet with different fractal dimensions resulting from different fabrication temperatures. In respect to the substrate fabrication temperatures the highest fractal dimension occurs at $T = 500\ ^0$C, with the value of about 2.65 (Fig.2).

Furthermore, the SiNW SERS substrate is a complex random structure and it would not be unexpected that it could also exhibit multifractal properties. Our preliminary multifractal analysis of substrate samples (see the Appendix D.) shows low to moderate degrees of multifractality. The involved (multi/bi) fractal dimensions do not differ much from corresponding D_g which represents the average value over all scales involved. The most important result of the preliminary fractal analysis is that there is no correlation between the degree of multifractality of our samples and the corresponding enhancement factors (the corresponding regression coefficient $R^2 = 0.1242$). Thus, further multifractal analysis is beyond the scope of this paper.

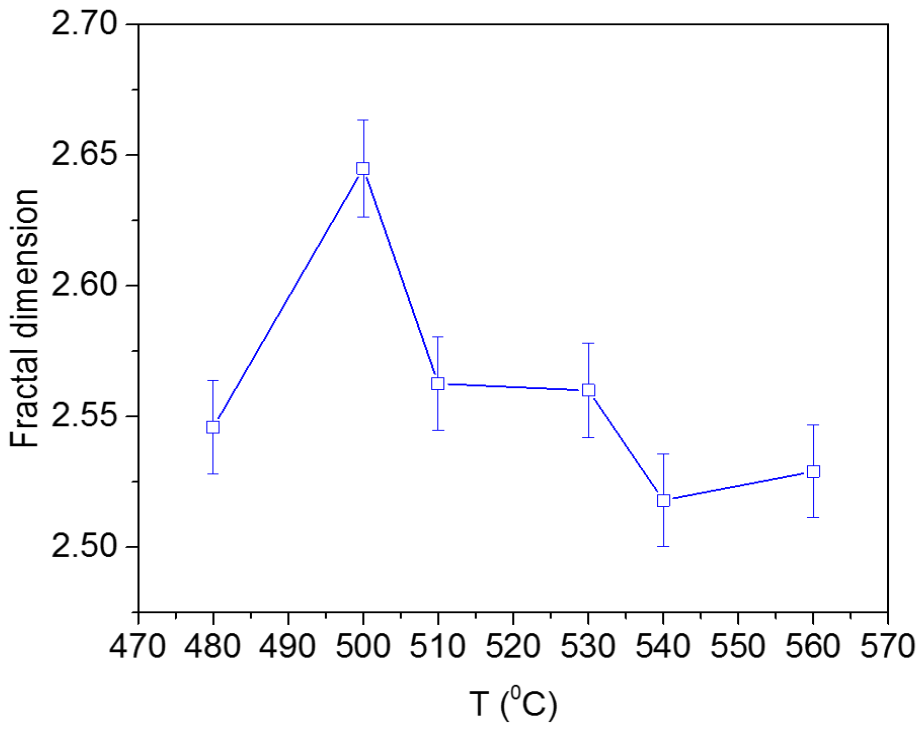

Fig. 2. Fractal dimensions of SiNWs substrates *vs*. fabrication temperature. Fractal dimensions of the substrates (identified by the fabrication temperature) were inferred from the corresponding grey-scale SEM images. The symbols represent average values and the error bars represent the corresponding standard deviations.

In light of the fact that the structures with lack of translational invariance prevent usual wave propagation and promote plasmonic wave localization within fractals resulting in exceptional SERS enhancement the lacunarity analysis of synthetized substrates is of high relevance for our study. Lacunarity is a concept distinct and independent from the fractal dimension and needs more than one numerical variable to be fully determined. Lacunarity is strongly related to the size distribution of the "holes" (voids) on the fractal structure and to its deviation from translational invariance. At a given scale, low lacunarity indicates homogeneous and transitionally invariant structure because all gap/voids sizes are of similar size, whereas objects of high lacunarity are heterogeneous and not transitionally invariant. However, it is important to note that high-lacunarity objects which are heterogeneous at small scales can be quite homogeneous at larger scales or vice versa. In other words, lacunarity is a scale-dependent measure of the spatial complexity of patterns [33, 34]. Hence, as a scale-dependent quantity the

lacunarity is usually presented as a lacunarity curve representing values of lacunarity *vs*. sampling window size (c.f. Fig. 3a). We determined the substrates' lacunarities from the corresponding SEM images following the procedure outlined in the Methods. The representative results of lacunarity analysis of grey-scale SEM images are presented in Fig. 3a, where the plot of average lacunarity $\Omega\lambda$ of grey-scale SEM images *vs.* window sampling element size is depicted.

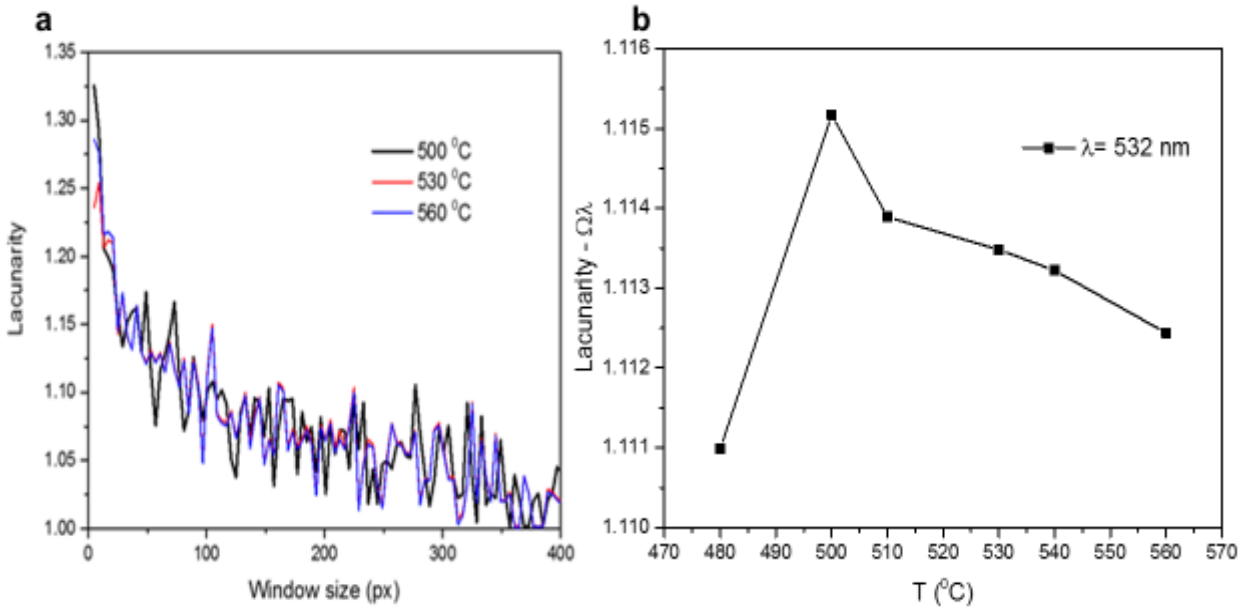

Fig. 3. Lacunarity of SiNWs SERS substrates. (**a)** Representative lacunarity curves of SiNWs substrates (identified with the fabrication temperature) *vs*. sampling window size (in pixels). Note that 1px = 6.13nm. (**b)** Average substrate lacunarity inferred from grey scale SEM images at sampling window sizes corresponding to the incident wavelength (532 nm) *vs.* substrate fabrication temperature.

Inspection of lacunarity curves depicted in Fig.3a shows that the lacunarity increases nearly exponentially with a decrease of the sampling window size and exhibits considerable fluctuations at greater sampling window sizes (> 50px). Since the lacunarity is a scale dependent quantity it is necessary to consider lacunarity at relevant scales i.e. these compatible with the involved wavelengths. Generally, strong light scattering occurs when the dimensions of a structural inhomogeneity are compatible with the effective wavelength of light propagating in the medium. The lacunarities of investigated substrates (identified by the fabrication temperature) at

sampling window sizes corresponding to the incident wavelength are depicted in Fig.3b. The maximum of lacunarity indicating relatively lower translational invariance of the substrate structure occurs for substrate manufactured at T = 500 ^{0}C with fractal dimension D_g = 2.65.

3.2. Analysis of enhancement of Raman scattering (SERS) in the fractal SiNWs substrates

We quantified the enhancement performances of fractal SiNWs substrates with SERS measurements performed on a Raman spectrometer in micro-single configuration with 532 nm excitation and using ethanol solution of mercaptophenylboronic acid (4-MPBA) as an analyte as described in the Methods.

The assemblies of nanostructures with fractal properties, whether ordered or disordered, profoundly influence the light transport inside the materials and, consequently, their optical properties, in particular the light scattering [1–5, 18]. When compared to non-fractal structures, where the surface plasmon modes are delocalized over a longer range, electromagnetic field enhancement in fractal structures due to the localization of plasmonic waves within fractals can be greater by an order of magnitude [35]. The localization occurs essentially by the confinement of local modes within the metal nanostructure, leading to a strong enhancement in the local plasmon intensity. In that context a "hot spot" is defined as a junction or close interaction of two or more plasmonic objects where at least one object has a small radius of curvature on the nm scale [36]. Hot spots are formed due to the collective and phase coherent excitation of localized surface plasmon resonance. The structural network of hot spots concentrates an incident electromagnetic field and effectively amplify the near field between and around the nanostructures. The intensity of surface-enhanced light scattering at a hot spot scales with the fourth power of the local field enhancement at the metal surface [37]. Moreover, the fractal geometry of such a system results in a scale-free localization, *i.e*. hot spots exist on all size scales ranging from those of the nanoscale components of the system to that of the entire structure. Also the size of the hot spots fluctuates widely across the structure. Altogether, in effect the overall enhancement should be structure dependent**.**

We have indeed observed such structure dependent enhancement of the spectral intensity as illustrated by SERS spectra of 10^{-3} M MPBA recorded at different fractal SiNWs substrates as depicted in Fig. 4. The 4-MPBA SERS spectral band assignment, not relevant for the present considerations, is given in the Ref. [38].

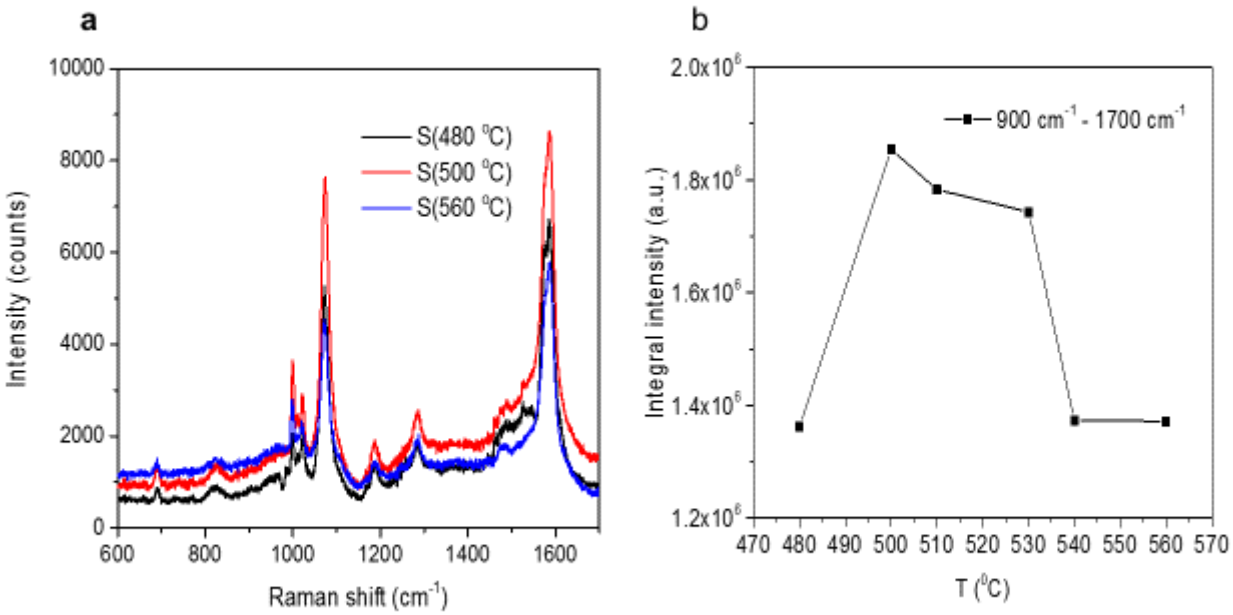

Fig. 4. Enhancement of SERS spectra. (**a)** Representative SERS spectra of 10^{-3} M MPBA recorded with the same experimental parameters at different SiNWs substrates *S(T)* designated by the corresponding fabrication temperature. (**b)** The integral intensity of 10^{-3} M MPBA Raman spectra in the relevant spectral range 900 cm^{-1} - 1700 cm^{-1} *vs*. the fabrication temperature of randomly oriented SiNWs mesh substrates.

From Fig. 4b, it can be clearly seen that the SERS intensity highly depends on substrate structure and that the highest integral SERS intensity is obtained using the substrate fabricated at *T*=500 ^{0}C. Such, substrate's structure dependent, intensity variation was also observed for single line intensities of principal Raman lines situated at ~ 1074 cm^{-1} and ~ 1585 cm^{-1}. This indicates that the enhancement process is independent of the specific molecular vibration, represented by its characteristic Raman shift, but rather related to the substrate structure. The same behavior was observed regardless of the investigated analyte concentration. It is obvious that, with all other parameters being equal, the intensity of Raman scattering depends on substrate structure which is

determined by the fabrication temperature and characterized by its fractal dimension and lacunarity. Mapping of the substrates responses (Fig. 2SI in the ESI) reveals relatively homogenous SERS response over the substrate surface with relative standard deviation SD ≤ 10%. It is commonly accepted that SD values around 20% indicate a fair grade of homogeneity in SERS detection [39, 40].

Next we discuss the interplay between long-range properties of nanostructured substrate, namely the fractal topology of the structure and the percolation phase transition, and short-range local features on the nanometer scale which are related to the distribution of inter particle/wire gaps (lacunarity) and strongly affect the local field enhancement. First, we examined the correlation between fractal dimensions of substrates D_g and corresponding spectral intensity enhancement. The dependence of integral SERS intensities on D_g for the relevant spectral band as well as the two main spectral lines cantered at ~ 1074 cm^{-1} and ~ 1585 cm^{-1} (cf. Fig. 4a) is depicted in Fig. 5a. The observed SERS intensities are well correlated with fractal dimension. The corresponding regression coefficients are 0.817, 0.879 and 0.855, respectively.

The enhancement factor (EF) calculated from SERS spectra for 10^{-3} M MPBA sample on the SiNWs substrates *vs*. corresponding fractal dimension is presented in Fig. 5b. The EF were calculated for Raman peak at ~1585 cm^{-1} (calculation details are described in ESI), and the enhancement is uniform over the whole surface, with a standard deviation of about 10%, as documented by mapping data presented in the ESI.

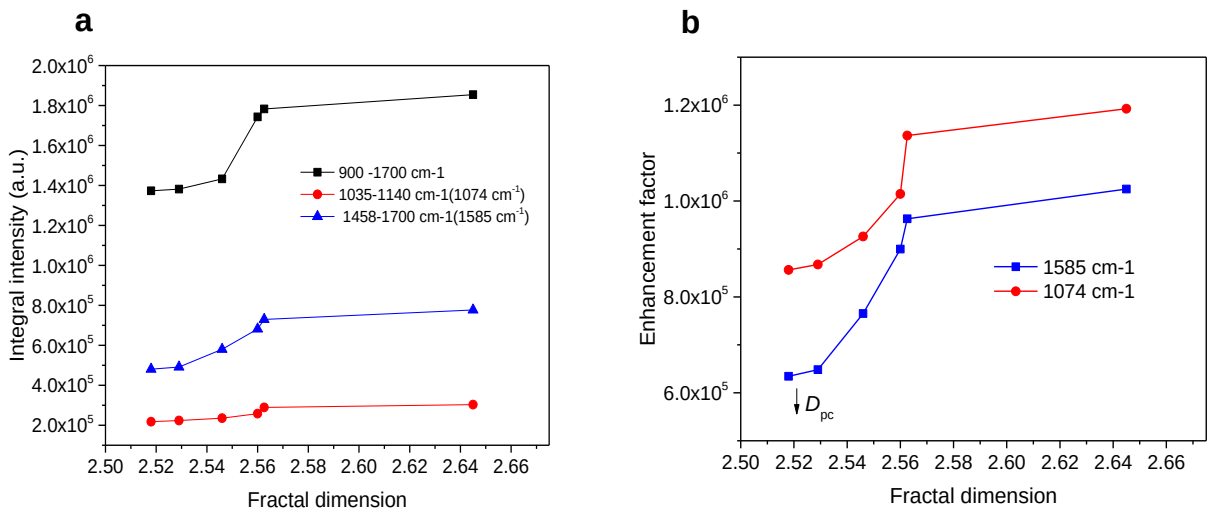

Fig. 5. Influence of substrate fractal dimension on Raman spectrum enhancement. (**a)** Integral Raman spectral band and line intensities of 10^{-3} M MPBA sample recorded at various substrates characterized with the corresponding fractal dimensions D_g. (**b)** Enhancement factor for principal SERS line at 1585 cm^{-1} *vs.* substrate's fractal dimension. D_{pc} denotes theoretical fractal dimension at the percolation threshold.

Inspection of plots of SERS intensity and enhancement factors *vs*. D_g (Fig. 5a and 5b) shows a threshold in the variation of the integral spectral intensities and a threshold in the corresponding EF occurring at about $D_g \approx 2.53$. After the threshold, SERS intensity and EF increase rapidly. For principal SERS line at 1585 cm^{-1} this rapid growth is confined to a narrow range of $2.54 < D_g < 2.56$ after the threshold value. In this range, a slight increase of D_g of only ~1% results in nearly doubling of enhancement factor. For $D_g > 2.57$ the spectral intensities and EF only slowly increase with a further increase of D_g.

The experimental data depicted in Fig.5, i.e. change of intensity/enhancement factor with change in fractal dimension, are excellently fitted with a sigmoidal-logistic growth model as illustrated in Fig. 6. Previously various sigmoidal growth models were extensively used in numerous studies of percolation such as e.g. investigation of the percolation threshold of electrical conductivity in polymer composites [41].

In our case the corresponding equation of a sigmoidal-logistic growth is given by:

$$Y = Y_0 + \frac{Y_m - Y_0}{1+(\frac{D}{D_0})^n} \quad (6)$$

Here, Y is the dependent variable (intensity, enhancement factor etc.), Y_0 is an initial/base value, Y_m is final value, D is fractal dimension, D_0 is point of maximal growth rate and n a slope factor.

Analysis of all fitted data, such as those depicted in Fig. 6 shows that the point of maximal growth rate D_0 of dependent variables (intensities and/or enhancement factors) is practically identical with value $D_0 = 2.555 \pm 0.003$, while the growth is confined to a very narrow D range. The values at 20% and 80% of corresponding maximal values $Y(20)$ and $Y(80)$ occur at $D = 2.546 \pm 0.005$ and $D = 2.563 \pm 0.003$. In application of sigmoidal-logistic growth to percolation problems it is often assumed that that the point of maximal growth rate (here D_0) corresponds to the percolation threshold [41].

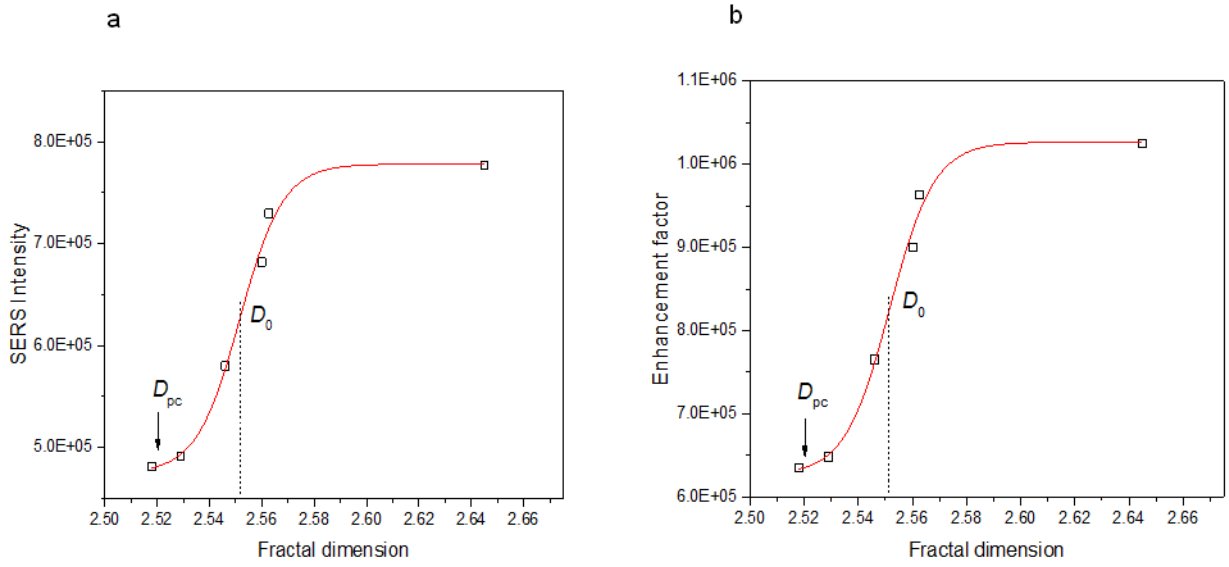

Fig. 6. **Fit of experimental data for principal SERS line at 1585 cm^{-1} *vs.* substrate's fractal dimension with sigmoidal-logistic growth model**. **(a)** SERS intensity and **(b**) the corresponding enhancement factor. Symbols denote experimental data and lines fit with the sigmoidal-logistic growth model**.** D_{pc} denotes theoretical fractal dimension at the percolation threshold and D_0 is point of maximal growth rate. $D_0 = 2.552$ and $R^2 = 0.9845$

Such experimentally observed behavior can be explained within the framework of the percolation theory [42]. Namely, the value of fractal dimension at the observed threshold of intensity/enhancement factor jump closely (within measurement uncertainty) corresponds to the theoretical percolation threshold in three dimensions (D_{pc} = 2.52) thus, indicating appearance of a connected, weakly correlated disordered structure [43]. Percolation, a second order phase transition, represents the basic model for a structurally disordered system. The percolation theory deals with development and growth of connectivity within structures, particularly aggregates and clusters. Percolation threshold is a mathematical concept in percolation theory, indicating the occurrence of a long-range connectivity in random systems. It is the critical value p_c of the occupation probability p, at which large structures/clusters and long-range connectivity first appears. Theoretically, when p approaches the critical point nanowire clusters grow and merge together to form an infinite connected cluster. The fractal dimension D_{pc} of a percolating system depends only on (Euclidian) dimensionality d of the system and not on details of local structure geometry [40]. The theoretical fractal dimensions at percolation thresholds for systems in three and two dimensions are 2.52 and 1.89, respectively.

Here, it is worth noting that the generated percolation structure dramatically modifies characteristics of the material: a structural phase transition occurs, the correlation length jumps, order parameter and the object symmetry and other parameters are changing, thus leading to changes in physical-chemical and mechanical characteristics. Such structures substantially modify the diffusion and conductivity processes, affect the kinetics of chemical reactions, define the mechanical strength and corrosion resistance, and lead to other phenomena [44-46]. Hence, we may conclude that in our case the significant increase of SERS occurs after the onset of percolation which results in a connected, weakly correlated structure. This is in line with theoretical prediction that the „hot spots" are much stronger at percolation threshold [47] and recent finding that for the gold films the maximum SERS signal was observed near the percolation threshold [48].

The structures with fractal dimensions below the percolation thresholds are not fully connected in a sense that they do not span the considered space. The crossing of the nanowires in the percolated SiNWs network leads to coupled plasmon behavior that spatially extends to encompass the regions between and significantly beyond the wires [49]. This strong coupling,

and porous percolated structure allowing more molecules to enter this high electric field regions result in a significant enhancement of the SERS effect and sensitivity.

The next relevant feature of the substrate's structure influencing the light enhancement is its lacunarity. Generally, strong light scattering occurs when the dimensions of a structural inhomogeneity are compatible with the effective wavelength of light propagating in the medium. Since the lacunarity is a scale dependent quantity it is necessary to consider lacunarity at relevant scales i.e. these compatible with the involved wavelengths. Since in our Raman measurements the laser wavelength is 532 nm the relevant scale – window size at which interaction takes place, i.e. lacunarity corresponding to inhomogeneity which laser "sees" is 532 nm.
Although the differences in lacunarity between the considered substrates are not very high their influence on the enhancement of the scattered intensity is significant. Since the relation between lacunarity and fractal dimension is a non-linear one (cf. Fig.8) the influence of lacunarity on signal enhancement is more complex. Consequently the behavior of enhancement factor with variation of lacunarity is somewhat different in comparison to the variation with corresponding fractal dimension. This is clearly seen from plots of the SERS intensities *vs*. lacunarity at the excitation wavelength presented in Fig. 6. For the excitation wavelength (532 nm) the SERS intensity *vs*. lacunarity exhibits similar behavior as observed in intensity vs. D_g plots (c.f. Fig. 5a), namely occurrence of intensity jump at samples with lacunarity $\Omega\lambda \approx 1.113$ ($D \approx D_{pc}$) and maximum for substrate with the highest lacunarity fabricated at 500^0C ($D = 2.65$). The correlation coefficients between lacunarity at excitation wavelength and the integral intensities of SERS spectral band and lines depicted in Fig. 7 are relatively high, with values 0.769, 0.745 and 0.668, respectively.

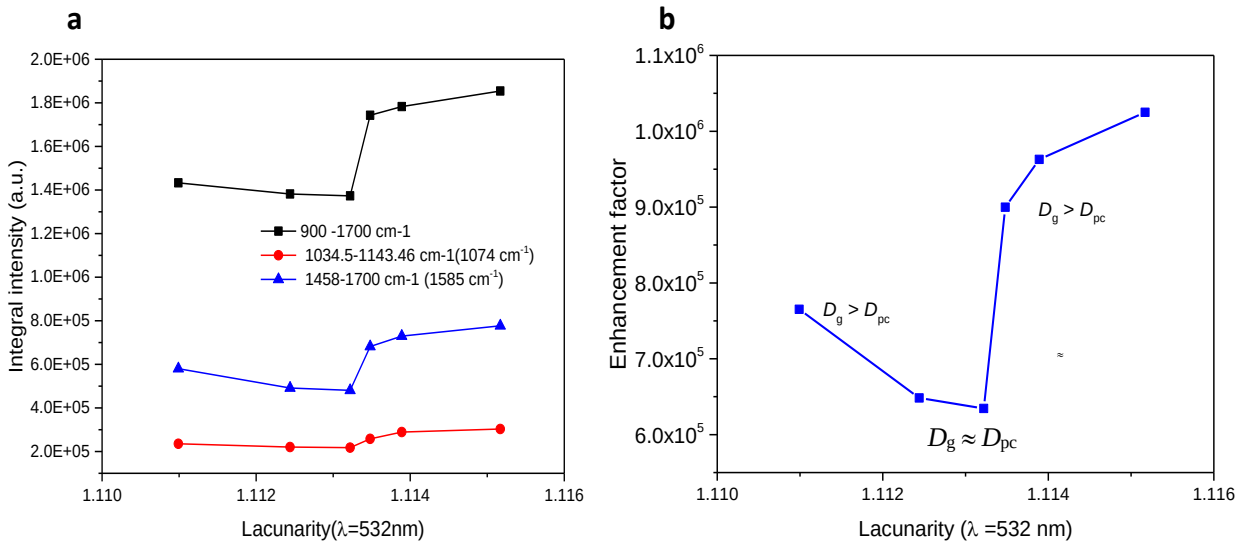

Fig. 7. Influence of substrate lacunarity at the excitation wavelength on Raman spectrum enhancement. (**a)** Integral Raman spectral band and line intensities of 10^{-3} M MPBA sample recorded at various substrates characterized with the corresponding lacunarity at the excitation wavelength (532 nm). (**b)** The enhancement factor for principal SERS line at 1585 cm^{-1} *vs.* substrate's lacunarity. The relative values of corresponding fractal dimensions D_g in respect to the value of fractal dimension at the percolation threshold D_{pc} are shown along the respective measurement points.

On the other hand, as expected theoretically lacunarity and fractal dimension are not correlated (c.f. Fig. 8), since, as mentioned before, lacunarities of structures with the same fractal dimension can be significantly different (or vice versa). Hence, we are dealing with two relatively independent parameters governing the enhancement of scattered intensity. Consequently this is manifested as a difference in respective regression coefficients as documented above. Now, in order to get a deeper insight into the intricate interplay between substrate's fractal dimension and lacunarity resulting in significant surface enhanced Raman scattering in Fig. 8 we put together all relevant information regarding the fractal dimensions, lacunarities and the SERS intensities.

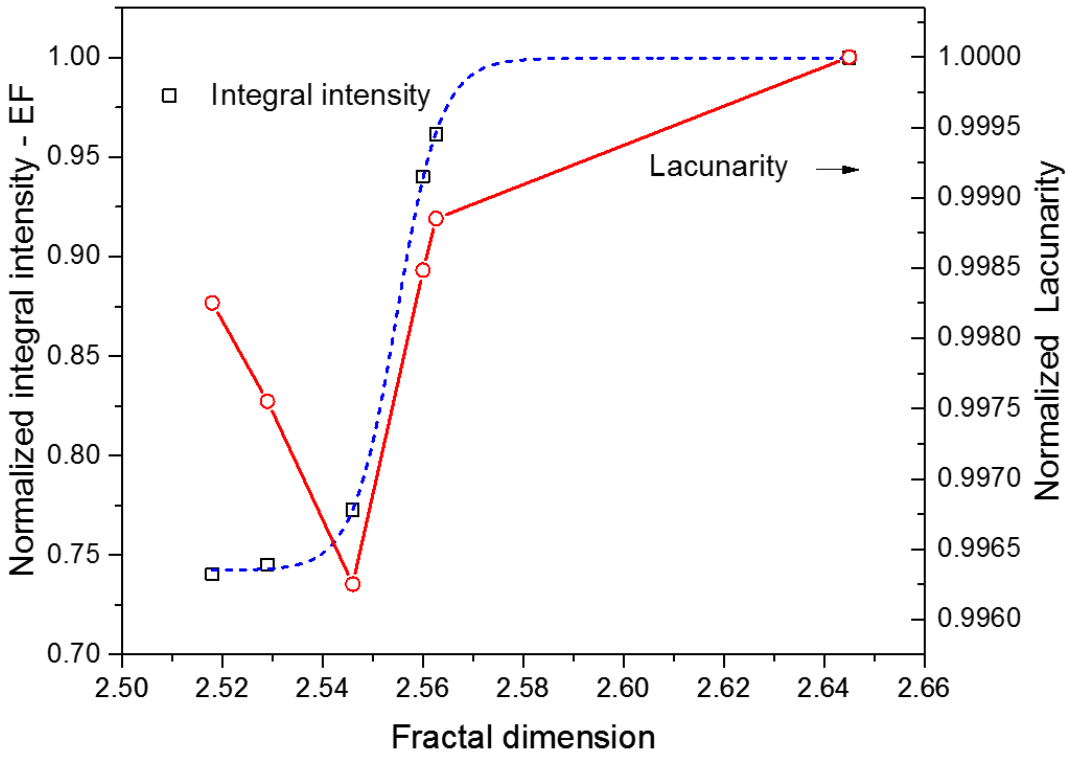

Fig. 8. Influence of substrate's fractal and lacunar characteristics on enhancement of Raman intensity. Normalized integral intensity (and EF) of considered SERS spectral band (900 cm^{-1} - 1700 cm^{-1}) of 10^{-3} M MPBA samples and normalized lacunarity corresponding to excitation wavelength *vs*. substrate's fractal dimension. *Note*: the values of normalized EF are identical to normalized intensity values. Symbols represent measurement points and dashed line a sigmoidal fit of normalized intensity (EF), D_0 = 2.554, D (10%) = 2.545.

Inspecting the plots in Fig. 8 we can see, aside from afore discussed change of enhancement with D, also a considerable dynamics and distinctive change of lacunarity with increase in fractal dimension. Initially as D_g increases the lacunarity decreases due to increase of connectivity of nanowires and increased size of connected clusters resulting in narrowing the size distribution of voids, i.e. the lacunarity. At the percolation threshold restructuring (a geometrical phase transition) occurs resulting in full connectivity and relative minimum of lacunarity ("neutral lacunarity"), compliant with theoretical predictions [50, 51]. Subsequent increase of lacunarity within the structure leads, due to decrease/lack of translational invariance, to enhanced scattering.

Thus, relatively high lacunarity per se does not result in significant enhancement of the scattering. Rather a fully percolated structure together with relatively high lacunarity is required for a significant increase of SERS and high enhancement factors. Furthermore, since the lacunarity is a scale dependent quantity it is different for different probing/excitation light wavelengths. Hence a corresponding pattern/distribution of localized optical excitations *i.e.* hot spots spatial positions will be strong function of the wavelength. This effect was indeed observed previously although it was not related to lacunarity [52].

3. Conclusions

We have investigated the influence of fractal and lacunar structural properties of randomly oriented Si-nanowires substrate on the enhancement of SERS. To that purpose we have synthetized SERS substrates with different fractal/lacunar structures using VLS approach. We discussed the involved interplay between long-range properties of nanostructured substrate, namely its fractal topology, and short-range local features on a nanometer scale related to the distribution of inter-wire gaps (i.e. lacunarity) which strongly affect the local field enhancement, altogether precipitating in significant increase of SERS. The results of our investigation have shown that:

- Fractal dimension and lacunarity of nanostructured SERS substrates have a profound influence on SERS enhancement.
- There exists a strong correlation between the enhancement of Raman scattering intensity and the corresponding fractal dimension and lacunarity of the considered substrate. No correlation between the degree of multifractality and the enhancement factor has been found.
- The observed correlations are explained within the framework of the percolation theory. Namely, we have shown that the observed abrupt increase in SERS occurring in SiNW structure with $D > D_{pc}$ is result of a second order phase transition – percolation;

- The occurrence of percolation, identified with corresponding fractal dimension D_{pc}, results in jump of enhancement factor. Thus, percolated nanostructured substrates exhibit high SERS response;
- Other parameter significantly influencing enhancement is lacunarity which is related to the size distribution of inter nanowire gaps and consequently influences distribution of localized optical excitations *i.e.* "hot spots" spatial positions
- The highest Raman scattering enhancement was obtained for a substrate with percolated structure lacking the translational invariance as indicated by a high lacunarity.
- Furthermore, for a percolated structure a strongly enhanced Raman emission, due to multiple scattering processes, is shown to depend on the excitation wavelength resonantly matching the heterogeneity sizes of the SiNWs fractal arrangement characterized with high lacunarity.
- The highest enhancement of Raman scattering intensity was observed for SiNWs substrate fabricated at 500 ^{0}C with D_g = 2.65 and lacunarity $\Omega\lambda$ = 1.115 at the excitation wavelength (532 nm).

As the enhancement of Raman scattering depends on fractal and lacunar characteristics of the substrate that are in turn determined by synthesis/annealing temperature, the selection of the processing temperature allows the design of a substrate with optimal performances. The observed performances make this novel random fractal architecture of SiNW-mesh very promising and reliable substrate for SERS. Altogether, the results of this study represent significant advancement in understanding of influence of fractal and lacunar features of a nanostructured substrates on SERS.

Corresponding Authors

* E-mail: Dubravko.Risovic@irb.hr

* E-mail: Hrvoje.Gebavi@irb.hr

Acknowledgements

This work has been supported by SAFU, project KK.01.1.1.01.0001 and by Croatian Science Foundation under the project (IP-2014-09-7046).

REFERENCES

[1] P.L. Stiles *et al.* Surface-enhanced Raman spectroscopy, Annu. Rev. Anal. Chem, 1 (2008**)** 601-626. https://doi.org/10.1146/annurev.anchem.1.031207.112814

[2] E. Le Ru and P. Etchegoin Eds., Principles of Surface-Enhanced Raman Spectroscopy: and related plasmonic effects, Elsevier Science: Oxford, 2008. ISBN**:** 9780444527790

[3] P.A. Mosier-Boss, Review of SERS Substrates for Chemical Sensing. Nanomaterials, *7* (2017**)** 142. https://doi.org**/**10.3390/nano7060142

[4] M.I. Stockman., V.M. Shalaev, M. Moskovits, R. Botet and T.F. George, Enhanced Raman scattering by fractal clusters: Scale-invariant theory, Phys. Rev. B 46 **(**1992) 2821–2831. https://doi.org/10.1103/PhysRevB.46.2821

[5] A. V. Markel, M. V. Shalaev, B. E. Stechel, W. Kim and L. R. Armstrong, Small-particle composites. I. Linear optical properties, Phys. Rev. B, 53 (1996) 2425–2436. https://doi.org/10.1103/PhysRevB.53.2425

[6] L. Mikac *et al*., Metal Nanoparticles Deposited on Porous Silicon Templates as Novel Substrates for SERS, Croat. Chem. Acta. 88 (2015) 437–444. https://doi.org/10.5562/cca2769

[7] X. Sun, L. Lin, Z. Li, Z. Zhang and J. Feng, Fabrication of silver-coated silicon nanowire arrays for surface-enhanced Raman scattering by galvanic displacement processes, Appl. Surf. Sci. 256 (2009), 916-920. https://doi.org/10.1016/j.apsusc.2009.08.085

[8] H. Gebavi *et al*., Silicon Nanowires Substrates Fabrication for Ultra-Sensitive Surface Enhanced Raman Spectroscopy Sensors, Croat. Chem. Acta, 90(2) (2017) 259–262. https://doi.org/10.5562/cca3127

[9] H. Gebavi *et al.*, Horizontal silicon nanowires for surface-enhanced Raman spectroscopy, Mater. Res. Express 5 (2018) 015015. https://doi.org/10.1088/2053-1591/aaa152

[10] B. Fan *et al.*, Silicon nanowire arrays coated with electroless Ag for increased surface-enhanced Raman scattering, Appl. Materials 3 (2015) 056101. https://doi.org/10.1063/1.4921040

[11] V. S. Vendamani *et al*., Three-dimensional hybrid silicon nanostructures for surface enhanced Raman spectroscopy based molecular detection, J. Appl. Phys. 23 (2018) 014301. https://doi.org/10.1063/1.5000994

[12] J. Yang, J. B. Li, Q. H. Gong. J. H. Teng and M. H. Hong, High aspect ratio SiNW arrays with Ag nanoparticles decoration for strong SERS detection, Nanotechnology 25 (2014) 465707. https://doi.org/10.1088/0957-4484/25/46/465707

[13] A. Convertino and M. Luca, Disordered array of Au covered Silicon nanowires for SERS biosensing combined with electrochemical detection, Scientific Reports 6 (2016) 25099. https://doi.org/10.1038/srep25099

[14] M. L. Zhang *et al.*, High-Efficiency Surface-Enhanced Raman Scattering Substrate Based Silicon Nanowires Array Decorated with Silver Nanoparticles, J. Phys. Chem. C 114 (2010) 1969–1975. https://doi.org/10.1021/jp902775t

[15] M. S. Schmidt, J. Hübner and A. Boisen, A. Large Area Fabrication of Leaning Silicon Nanopillars for Surface Enhanced Raman Spectroscopy, Adv. Opt. Mater. 24 (2012) OP11–OP18. https://doi.org/10.1002/adma.201290051

[16] X.Yang, H. Zhong, Y. Zhu, J. Shen and C. Li, Ultrasensitive and recyclable SERS substrate based on Au-decorated Si nanowire arrays, Dalton Trans. 42 (2013) 14324–30. https://doi.org/10.1039/C3DT51686E

[17] E. Cara, L. Mandrile *et al.*, Influence of the long-range ordering of gold-coated Si nanowires on SERS, Scientific Reports 8 (2018) 11305. https://doi.org/10.1038/s41598-018-29641-x

[18] V. M. Shalaev and A. K. Sarychev, Nonlinear optics of random metal-dielectric films, Phys. Rev B, 57 (20), (1998), 13265-13288. https://doi.org/10.1103/PhysRevB.57.13265

[19] W. Kern, The Evolution of Silicon Wafer Cleaning Technology, J. Electrochem. Soc. 137(6) (1990) 1887-1892. https://doi.org/10.1149/1.2086825

[20] Fractal3e. (2011). Fractal analysis system for Windows –software download and documentation. Available online at: http://cse.naro.affrc.go.jp/sasaki/fractal/fractal-e.html (accessed March 2020).

[21] http://rsb.info.nih.gov/ij/plugins/fraclac/FLHelp/Introduction.htm (accessed Juni 2020). .

[22] http://gwyddion.net/ (accessed March 2020).

[23] D. Risović and Ž. Pavlović, Performance Assessment of Methods for Estimation of Fractal Dimension From Scanning Electron Microscope Images, Scanning 35 (2013) 402–411. https://doi.org/10.1002/sca.21081

[24] E. Hadzieva, *et al*. Review of the Software Packages for Estimation of the Fractal Dimension, in S. Loshkovska, S. Koceski (Editors): ICT Innovations 2015, Web Proceedings, ISSN 1857-7288 © ICT ACT http://ictinnovations.org/2015, 2015ICT

[25] A.P. Pentland, Fractal based description of natural scenes, IEEE Trans. Pattern Anal. Mech. Intell. 6 (1984) 661–674. https://doi.org/10.1109/TPAMI.1984.4767591

[26] M. Li J., Lu. Li, M.O. Lai and B. Ralph, Image-based fractal description of microstructures. Kluwer Academic Publishers: Boston 2003. ISBN 978-1-4020-7507-0

[27] B. Dubuc, S.W. Zucker., C.Tricot, J.F. Quiniou and D. Wehbi, Evaluating the fractal dimension of surfaces, Proc. R. Soc. London A 425 (1989) 113–127. https://doi.org/10.1098/rspa.1989.0101

[28] K. Falconer, Fractal geometry, mathematical foundations and applications. John Wiley and Sons, Inc.: Chichester, 1990. ISBN: 978-1-119-94239-9

[29] W.S. Chen, S.Y. Yuan and C.M. Hsieh, Two algorithms to estimate fractal dimension of gray-level images, Opt. Eng. 42 (2003) 2452–2464. https://doi.org/10.1117/1.1585061

[30] T.G. Smith Jr., G.D. Lange and W.B. Marks, Fractal methods and results in cellular morphology - dimensions, lacunarity and multifractals, Journal of Neuroscience Methods 28(2) (1996) 123-136. https://doi.org/10.1016/S0165-0270(96)00080-5

[31] R. E. Plotnick *et al*. Lacunarity analysis: A general technique for the analysis of spatial patterns, Phys. Rev. E 53 (1996) 5461-5468. https://doi.org/10.1103/PhysRevE.53.5461

[32] S. Mahović Poljaček, D. Risović, K. Furić and M. Gojo, Comparison of fractal and profilometric methods for surface topography characterization, Appl. Surf. Sci. 254 (2008) 3449–3458. https://doi.org/10.1016/j.apsusc.2007.11.040

[33] R. E. Plotnick, R. H. Gardner, and R. V. O'Neill, Lacunarity indices as measures of landscape texture, Landscape Ecology 8(3) (1993) 201-211. https://doi.org/10.1007/BF00125351

[34] Y. Quan, Y. Xu , Y. Sunand and Y. Luo, Lacunarity Analysis on Image Patterns for Texture Classification, IEEE Conference on Computer Vision and Pattern Recognition (2014) 160-167. https://doi.org/10.1109/CVPR.2014.28

[35] L. He, N.K. Kim, H. Li, Z. Hu, and M. Lin, Use of a Fractal-like Gold Nanostructure in Surface-Enhanced Raman Spectroscopy for detection of selected food contaminants, J. Agric. Food Chem. 56 (2008) 9843–9847. https://doi.org/10.1021/jf801969v

[36] S. L Kleinman, R. R. Frontiera, A.I. Henry, J. A.Dieringer, and R. P. Van Duyne, Creating, characterizing, and controlling chemistry with SERS hot spots. Phys. Chem. Chem. Phys., 15(1), (2013). 21–36. https://doi.org/10.1039/c2cp42598j

[37] P. Alonso-González, *et al*. Resolving the electromagnetic mechanism of surface-enhanced light scattering at single hot spots, *Nat. Commun.* **3,** 684 (2012) 1-7. https://doi.org/10.1038/ncomms1674

[38] Pham, X., Shim, S., Kim, T. *et al.*, Glucose Detection Using 4-mercaptophenyl Boronic Acid-incorporated Silver Nanoparticles-embedded Silica-coated Graphene Oxide as a SERS Substrate, Bio Chip J. 11(1) (2017) 46-56. https://doi.org/10.1007/s13206-016-1107-6

[39] X. Tang, W. Cai, L. Yang and J. Liu, Highly uniform and optical visualization of SERS substrate for pesticide analysis based on Au nanoparticles grafted on dendritic α-Fe_2O_3, Nanoscale, 5 **(**2013) 11193-11199 https://doi.org/10.1039/c3nr03671e

[40] J. Quan, J. Zhang, X. Qi, J. Li, N. Wang and Y.Zhu, A study on the correlation between the dewetting temperature of Ag film and SERS intensity, *Scientific Reports* 2017, **7**, *14771* https://doi.org/10.1038/s41598-017-15372-y

[41] M. Rahaman, A. Aldalbahi, P. Govindasami,N. P. Khanam, S. Bhandari, P. Feng and T. Altalhi, A New Insight in Determining the Percolation Threshold of Electrical Conductivity for Extrinsically Conducting Polymer Composites through Different Sigmoidal Models, Polymers 9 (2017**)** 527 https://doi.org/10.3390/polym9100527

[42] D. Stauffer and A. Aharony , Introduction to Percolation Theory; Taylor and Francis: London, 1992. https://doi.org/10.1201/9781315274386

[43] J. Zierenberg *et al.*, Percolation thresholds and fractal dimensions for square and cubic lattices with long-range correlated defects, Phys. Rev. E. 96 (2018) 062125. https://doi.org/10.1103/PhysRevE.96.062125

[44] A. Herega , Some Applications of the Percolation Theory: Brief Review of the Century Beginning, J. Mat. Sci. Engineering A. 5 (11-12), (2015) 409-414. https://doi.org/10.17265/2161-6213/2015.11-12.004

[45] P. Bonnet, D. Sireude, B. Garnier and O. Chauvet, Thermal properties and percolation in carbon nanotube-polymer composites, Appl. Phys. Lett. 91 (2007) 01910. https://doi.org/10.1063/1.2813625

[46] D. Risović, S. Frka and Z. Kozarac, The Structure of Percolating Lipid Monolayers, J. Coll. Interface Sci. 373 (2012) 116–121. https://doi.org/10.1016/j.jcis.2011.12.009

[47] Optical properties of nanostructured random media, Vladimir M. Shalaev Ed., Springer Verlag Berlin, Heidelberg 2002, ISSN 0303-4216, 454pp (p. 169) ISBN 3540449485,

[48] D. E. Tatarkin *et al*., Surface-Enhanced Raman Spectroscopy on Hybrid Graphene/Gold Substrates near the Percolation Threshold, Nanomaterials, 10 (2020) 164. https://doi.org/10.3390/nano10010164

[49] S. M. Prokes, O.J. Glembocki, R. Rendell and M. Ancona, Effect of crossing geometry on the plasmonic behavior of dielectric core/metal sheath nanowires, Appl. Phys. Lett. 90 (2007) 093105. https://doi.org/10.1063/1.3094129

[50] J.P. Hovi, A. Aharony, D. Stauffer, and B. B. Mandelbrot, Gap Independence and Lacunarity in Percolation Clusters**,** Phys. Rev. Letters, 77(5) (1996) 877-880 https://doi.org/10.1103/PhysRevLett.77.877

[51] B. B. Mandelbrot and D. Stauffer, Antipodal correlations and the texture (fractal lacunarity) in critical percolation clusters, J. Physics A 27(9) (1994). L237-L242. https://doi.org/10.1088/0305-4470/27/9/001

[52] S. Ducourtieux *et al*., Near-field optical studies of semicontinuous metal films, Phys. Rev. B, 64 (2001) 165403. https://doi.org/10.1103/PhysRevB.64.165403

APPENDICES

A. Decoration of SiNWs with Ag nano-particles

SiNWs were relatively uniformly decorated with Ag nanoparticles using Polaron E5000 sputter coater for several minutes under constant Ar flow. The representative SEM image of Ag-decorated SiNWs is presented in Fig. A.1

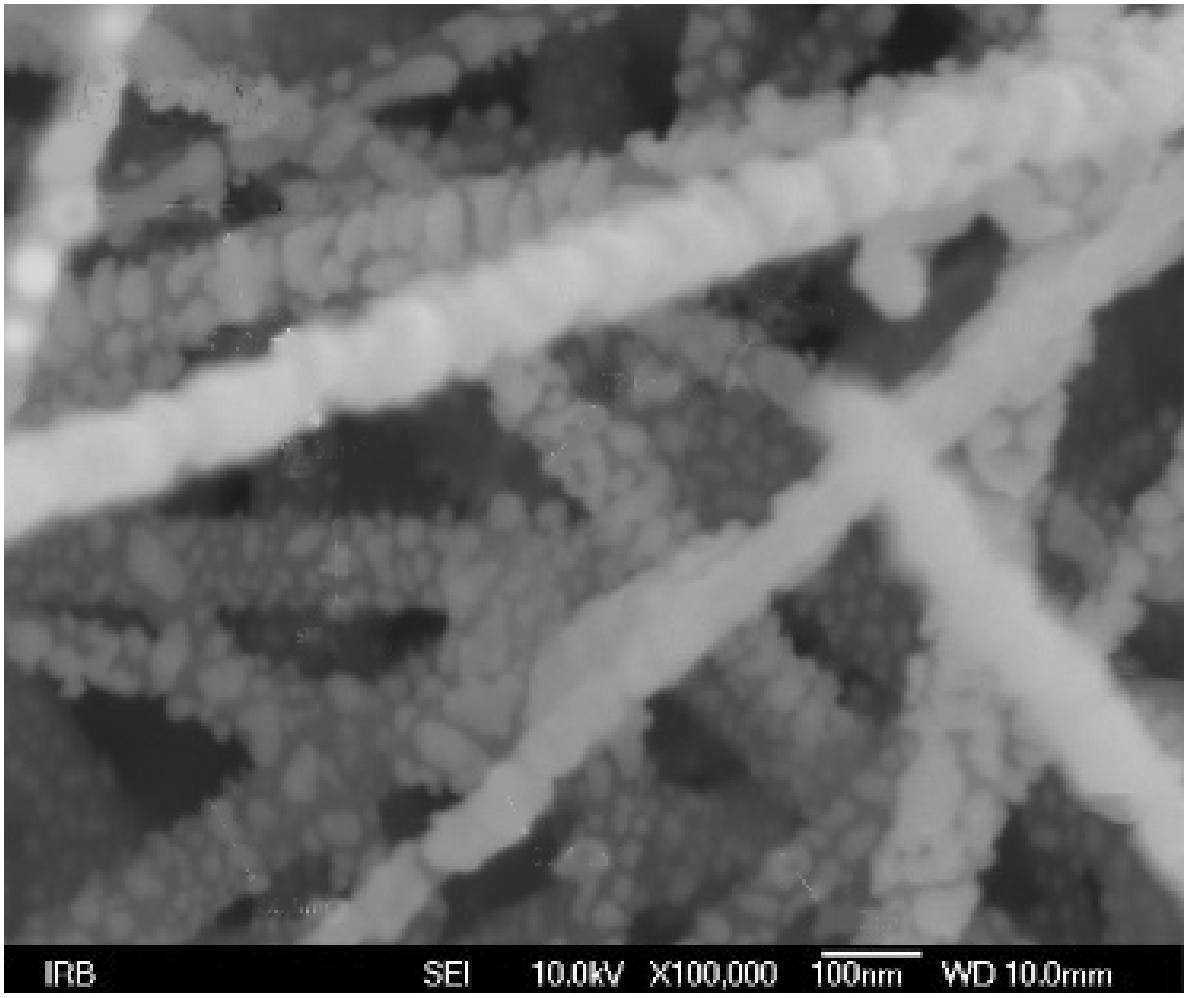

Fig. A.1 Ag-decorated SiNWs. Sputtering time 5 min. The approximate size of oval Ag nanoparticles is in the range of 20 – 30 nm

B. Raman mapping

The uniformity of SERS response over an active substrate is a crucial aspect in view of real applications. To evaluate it we mapped the SERS response across the representative substrate. The Raman spectroscopy measurements were performed on Jobin Yvon T64000 Raman spectrometer in micro-single configuration. The laser power at 532 nm on the sample with ~1μm spot size was ~1–2 mW. For all experiments, the 50x/0.75 objective was used. Exposition time was 20s for 1 scan.

The step size of the mapping was 10 μm, and one image contained the data from 100 scanning points. The SERS spectra of 100 points can integrate to generate artificial color images based on the intensity of a designated Raman peak. Results of mapping of 10^{-3} MPBA of 1073 cm^{-1} Raman band are presented in Fig. B.1

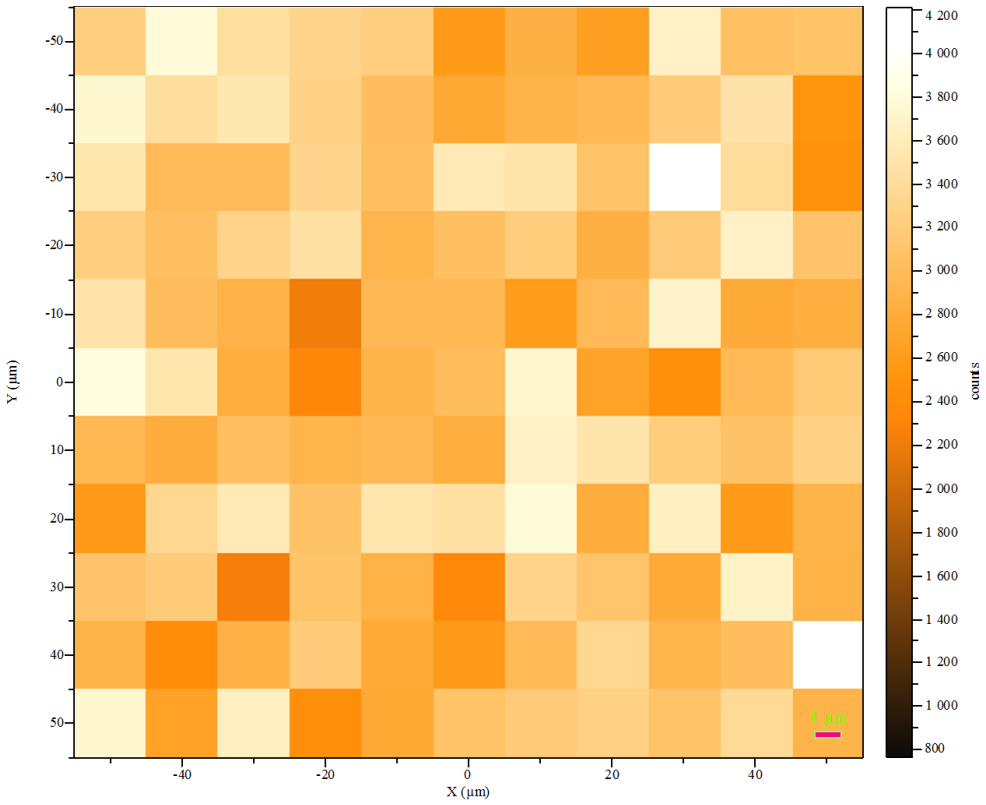

Fig. B.1. Mapping of 1073 cm^{-1} Raman band a 10^{-3} MPBA sample. Mapping features: 100 points, 10 μm step, 1 scan/point, 10 s/sc. Maximal intensity 4200 counts. Average intensity: 3420 ± 358 (≈ ± 10%) counts.

To assess the spatial homogeneity of a substrate the relative standard deviation (RSD) of signal obtained from multiple scanning is widely adopted in the SERS community [B.1, 2].

The average intensity inferred from substrate mapping using 10^{-3} MPBA and 1073 cm^{-1} Raman band is 3420 ± 358 counts. The corresponding RSD is $\approx$ 10%. This is a very good result since it is commonly accepted that RSD values around 20% indicate a fair grade of homogeneity in SERS detection [B.2-4].

References

[B.1] Fu, Q. *et al*. Highly Reproducible and Sensitive SERS Substrates with Ag Inter-Nanoparticle Gaps of 5 nm Fabricated by Ultrathin Aluminum Mask Technique. *ACS Appl. Mater. Interfaces* 7 (2015) 13322–13328, https://doi.org/10.1021/acsami.5b01524

[B.2] Peksa, V. *et al*. Testing gold nanostructures fabricated by hole-mask colloidal lithography as potential substrates for SERS sensors: sensitivity, signal variability, and the aspect of adsorbate deposition. *Phys. Chem. Chem. Phys.* 18 (2016) 19613–19620, https://doi.org/10.1039/C6CP02752K

[B.3] Wu, W. *et al*. Low-Cost, Disposable, Flexible and Highly Reproducible Screen Printed SERS Substrates for the Detection of Various Chemicals. *Sci. Rep.* 5 (2015) 10208, https://doi.org/10.1038/srep10208

[B.4] Luo, Z. *et al*. Net-like assembly of Au nanoparticles as a highly active substrate for surface-enhanced Raman and infrared spectroscopy. *J. Phys. Chem. A* 113 (2009) 2467–2472, https://doi.org/10.1021/jp810387w

C. Calculation of enhancement factor

SERS enhancement factor values were calculated from the average intensity of the appropriate MPBA spectral peak (~1585 cm^{-1}) measured in the three SERS experiments and corresponding peak of normal Raman measurements measured from a 1M aqueous solution of MPBA according to the method proposed in refs. [C.1-3]. Both SERS and Raman measurements were performed on Jobin Yvon T64000 Raman spectrometer in micro-single configuration under identical experimental conditions. The laser power@532 nm on the sample was ~1–2 mW. For all experiments, the 50x/0.75 objective was used. Exposition time was 20s for 1 scan.

The SERS enhancement factor (EF) is given by:

$$EF = \frac{I_{SERS}/N_{SERS}}{I_R/N_R} \quad \text{(C.1)}$$

where N_{SERS} and N_R represent the numbers of 4-MPBA molecules in the excitation volume measured using a SERS substrate and normal Raman, respectively. I_{SERS} and I_R are the signal intensities measured using SERS and normal Raman, respectively.

For SERS the excited volume was approximated as a cylinder with a base corresponding to the diameter of focused laser spot and a height corresponding to approximate focus depth of laser beam *Dof*.

The area of the focused laser spot S_{spot} can be calculated as

$$S_{spot} = \pi \frac{(1.22\lambda/NA)^2}{4}, \quad \text{(C.2)}$$

and the depth of focus is calculated from:

$$Dof = \frac{8\lambda}{\pi} NA^2 \quad \text{(C.3)}$$

where λ and *NA* are the laser wavelength and numerical aperture of the objective, respectively.

To measure the Raman intensity a drop (4μL) of 1M 4-MPBA was deposited on solid substrate, and then excited with a focused laser beam. The excitation volume was calculated from the laser spot size (Eq.C.2) and corresponding thickness of MPBA layer.

Then the number of the molecules was calculated using the excitation volumes and corresponding concentrations. Afterwards, using measured intensities the EF of the system can be easily calculated from (Eq.C.1). An enhancement factor of 1.02×10^6 was obtained for spectral peak at ~1585 cm^{-1}. This value is in the same order of magnitude of the one reported in ref. [C.2] on silver coated silicon nanopillars substrate.

References

[C.1] Le Ru, E. C., Meyer, M., Etchegoin, P. G., Le Ru, E. C. & Blackie, E. Surface Enhanced Raman Scattering Enhancement Factors: A Comprehensive Study. *J. Phys. Chem. C* 111 (2007) 13794–13803, https://doi.org/10.1021/jp0687908

[C.2] Schmidt, M. S., Hubner, J. & Boisen, A. Large area fabrication of leaning silicon nanopillars for Surface Enhanced Raman Spectroscopy. *Adv. Mater.* 24 (2012) 11–18, https://doi.org/10.1002/adma.201103496

[C.3] Hu, Y. S. *et al*. Enhanced Raman Scattering from Nanoparticle-Decorated Nanocone Substrates: A Practical Approach to Harness In-Plane Excitation. *ACS Nano* 4 (2010) 5721–5730 https://doi.org/10.1021/nn101352h

D. Multifractal analysis

The theoretical basis of multifractality can be found in the literature [D.1]; Block et al., 1990; Vicsek, 1992;Jestczemski and Sernetz, 1996] and is not covered here. Instead, we present a brief introduction necessary for understanding of results of our preliminary multifractal analysis.

For a homogeneous (monofractal) system, the probability (P) of a measure (here a number of pixels) appearing in a box varies with box size or scale L as

$$P(L) \sim L^{D} \tag{D.1}$$

where D is a fractal dimension. For heterogeneous (multifractal) systems, the probability within the ith region P_i scales as:

$$P_i(L) \sim L^{\alpha i} \tag{D.2}$$

where α_i is the Lipschitz-Holder exponent or singularity strength, characterizing scaling in the ith region.

The values of αi can be found at different positions within a distribution by the box counting technique. Then, the number of boxes $N(\alpha)$ where the P_i has singularity strengths between α and $\alpha + d\alpha$ is found to scale as [D.2]:

$$N(\alpha) \sim L^{-f(\alpha)} \tag{D.3}$$

Where $f(\alpha)$ can be defined as the fractal dimension of the set of boxes with singularities α.

$$\alpha(q) = \frac{\sum_{i=1}^{N_\tau} \mu_i \ln P_i}{\ln L}$$

$$f(\alpha) = \frac{\sum_{i=1}^{N_\tau} \mu_i \ln \mu_i}{\ln L} \qquad \text{(D.4)}$$

μ = mean value of the probability distribution at some L

A homogeneous fractal exhibits a narrow $f(\alpha)$-spectrum, whereas the opposite is true for an heterogeneous fractal.

The spectrum width or degree of multifractality is defined as

$$\Delta f(\alpha) = \alpha_{max} - \alpha_{min}. \qquad \text{(D.5)}$$

This is illustrated in Fig D.1 where representative $f(\alpha)$-spectra for samples with low and moderate multifractality are depicted. The corresponding degrees of multifractality $\Delta f(\alpha)$ for substrates 480^0C and 500^0C are 0.39 and 0.80, respectively.

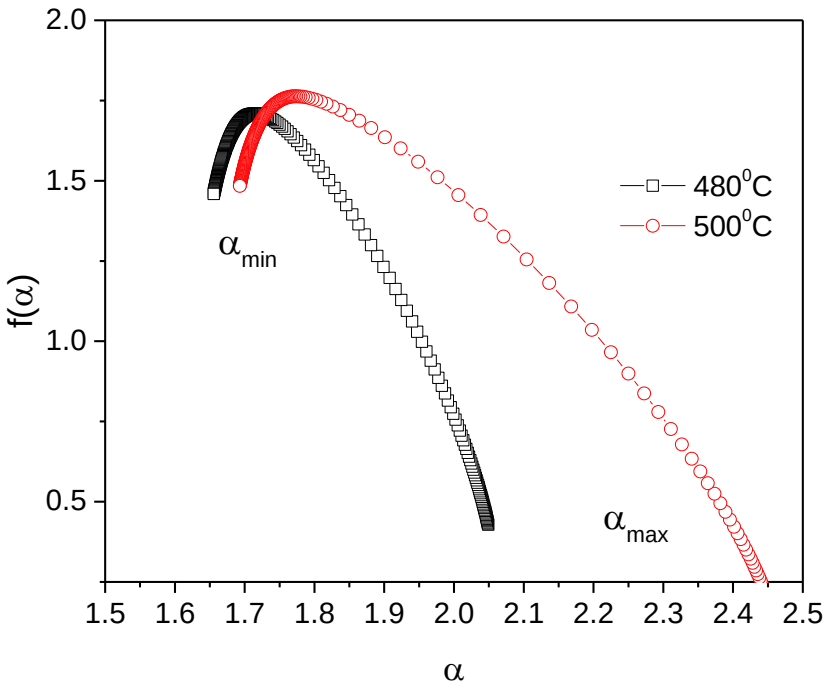

Fig. D.1 Multifractal spectrum for samples 480^0C and 500^0C with low and moderate multifractality, respectively. Respective degrees of multifractality $\Delta f(\alpha)$ are 0.39 and 0.80

Calculated degrees of multifractality for all investigated samples are depicted in Fig. D.2. The highest degree of multifractality (0.81) is obtained for substrate 500^0C, while other substrates exhibit significantly lower $\Delta f(\alpha)$ with average value 0.52 ± 0.1

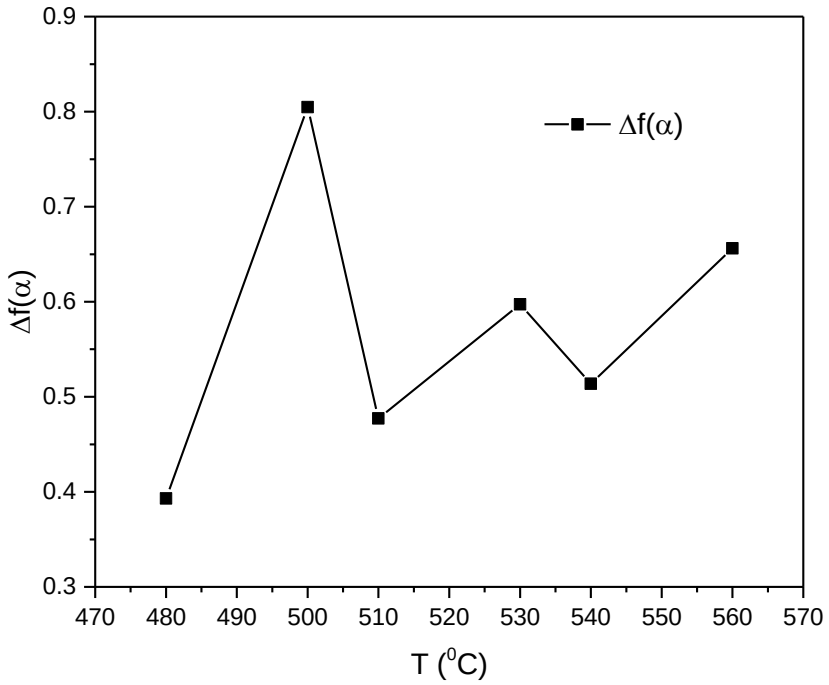

Fig. D. 2 Degrees of multifractality $\Delta f(\alpha)$ for all investigated samples identified with corresponding manufacturing temperature.

The most important result of our preliminary multifractal analysis is that there is no correlation between degree of multifractality of investigated substrates and corresponding enhancement factors. The regression coefficient $R^2 = 0.1242$. This could be readily concluded inspecting Fig. D.3 depicting Raman enhancement factor *vs*. $\Delta f(\alpha)$.

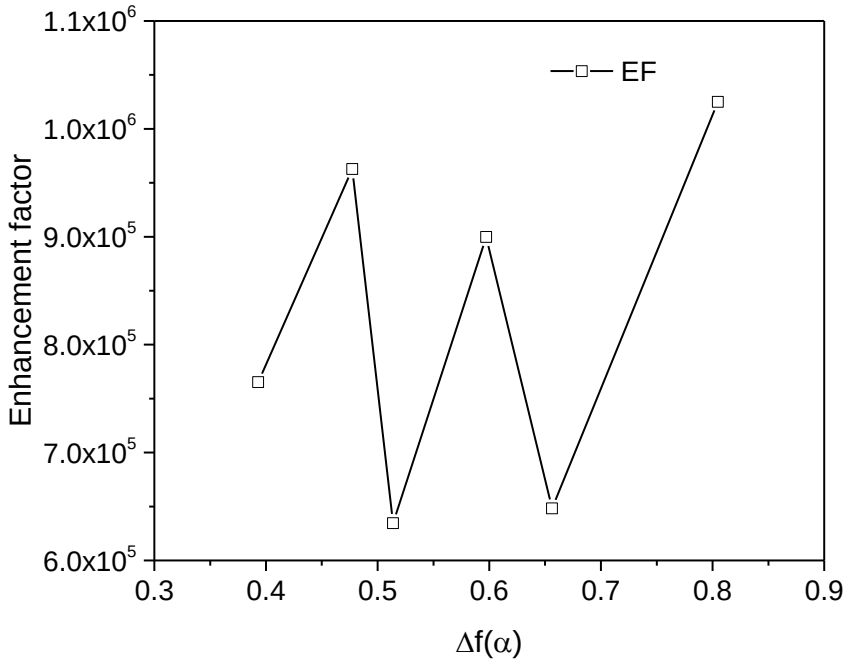

Fig. D. 3 The enhancement factor *vs.* degree of multifractality of the investigated substrates

Furthermore, multifractal sets can also be characterized on the basis of the generalized dimensions *Dq*, of the *q*th moment orders distribution, defined as [D.3, D.4]:

$$D_q = \frac{1}{q-1} \lim_{L \to 0} \frac{\log[\mu(q,L)]}{\log[L]} \quad \text{(D. 6)}$$

where μ(*q*, *L*) is the partition function that scles as

$$\mu(q, L) \sim L^{\tau(q)} \quad \text{(D. 7)}$$

Here τ(q) is the mass or correlation exponent of the qth moment order *q*.

Thus, the parameter *q* is a kind of a resolution parameter that enhances the regions corresponding to higher μ_ε values for positive values of *q*, and the regions of lower μ_ε values for negative values of *q*. Regarding the relation between multifractality and moment order *q* the curve f(α) is convex

with a single inflection point at the maximum with $q = 0$;) for $q = \pm\infty$, the slope is infinite and $\alpha_{min} = D_{+\infty}$, $\alpha_{max} = D_{-\infty}$. More rigorous discussion can be find in the literature [D.4]

The illustrative plots of D_q *vs.* q for samples 500^0C and 560^0C exhibiting different degrees of multifractality (0.80 and 0.65, respectively) are shown in Fig. D.4 below.

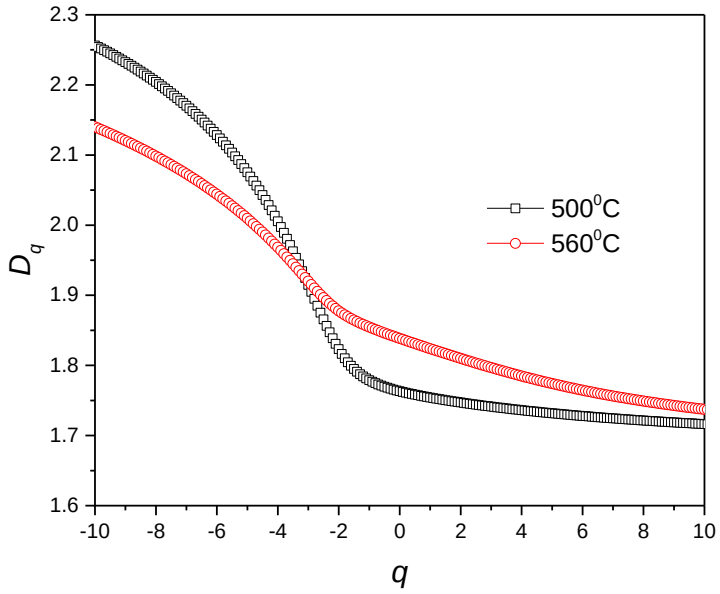

Fig. D.4 Generalized dimension *Dq vs. q* for structures with different degrees of multifractality. The sigmoidal curve corresponds to a structure with higher degree of multifractality and a more flat curve to a structure with lesser multifractality

Without going into the details plot of *Dq* vs. q is more or less a flat curve for monofractals and sigmoidal around $q = 0$ for multifractal structure, while a linear relationship between $\tau(q)$ and q implies a single fractal system characterized by one scaling exponent (homogeneous fractal).

On the other hand, variable slopes in a $\tau(q)$ *vs.* q relationship are indicative of a multifractal (heterogeneous) system [D.5]). A special case of the latter systems is the bifractal distribution, defined by two slopes dominating a $\tau(q)$ *vs.q* plot and related to different fractal dimensions. This is the case with our samples as clearly seen from representative plot of $\tau(q)$ *vs.* q (Fig. D.5). Here, the two ranges of $\tau(q)$ with different slopes corresponding to two different fractal dimensions can be easily identified. The crossover occurs at length scales of about 200 nm. Additional insight

into the scale at which crossover occurs could be provided by analysis of the auto-correlation length, since the autocorrelation function describes how well an image correlates with itself under conditions where the image is displaced with respect to itself in all possible directions [D.5, 6].

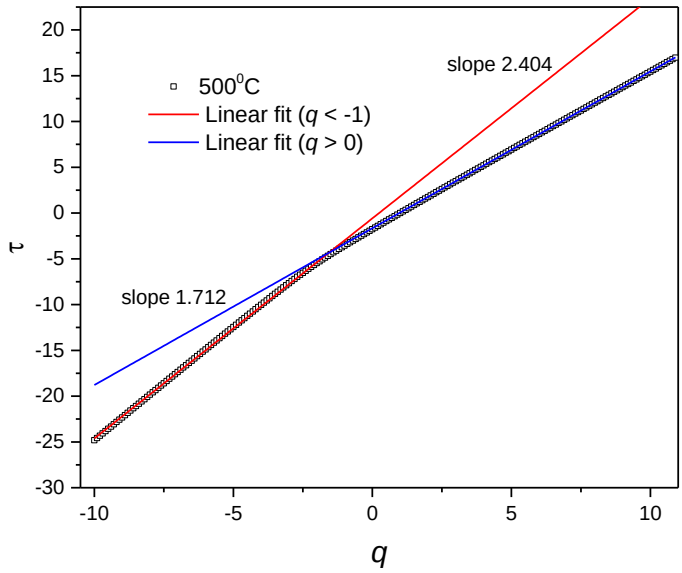

Fig. D.5 $\tau(q)$ *vs.* q for sample 500^0C ($\Delta f(\alpha) = 0.8$). Two different slopes of the plot in regions $q < 0$ and $q > 0$ are related to two different fractal dimensions. The crossover occurs approximately at about 200nm.

References:

[D.1] Chhabra, A.B., and R.V. Jensen Direct determination of the f(α) singularity spectrum. Phys. Rev. Lett. 62 (1989) 1327–1330. https://doi.org/10.1103/PhysRevLett.62.1327

[D.2] Chhabra, A.B., C. Meneveu, R.V. Jensen, and K.R. Sreenivasan, Direct determination of the f (α) singularity spectrum and its application to fully developed turbulence. Phys. Rev. A 40 (1989) 18. U.S. Gov. Print Office, Washington, DC. 5284–5294. https://doi.org/10.1103/PhysRevA.40.5284

[D.3] Hentschel, H.G.E., and I. Procaccia, The infinite number of generalized dimensions of fractals and strange attractors. Physica D 8(1983) 435–444. https://doi.org/10.1016/0167-2789(83)90235-X

[D.4] JM. Barbaroux, F.Germinet and S. Tcheremchantsev, Generalized fractal dimensions: equivalences and basic properties, J. Math. Pures Appl. 80, 10 (2001) 977–1012 https://doi.org/10.1016/S0021-7824(01)01219-3

[D.5] Machs, J., F. Mas, and F. Sagues, Two representations in multi fractal analysis. J. Phys. A: Math. Gen. 28 (1995) 5607–5622. https://doi.org/10.1088/0305-4470/28/19/015

[D.6] R.P. Heilbronner, The autocorrelation function: an image processing tool for fabric analysis, Tectonophysics 212 (1992) 351–370,

https://doi.org/10.1016/0040-1951(92)90300-U

[D.7] Marteau, J., and M. Bigerelle. "Relation between surface hardening and roughness induced by ultrasonic shot peening." *Tribology International* 83 (2015): 105-113. https://doi.org/10.1016/j.triboint.2014.11.006

Influence of fractal and lacunar characteristic of a nanostructured substrate on SERS enhancement

Dubravko Risović[*1], Hrvoje Gebavi[*1] and Mile Ivanda[1]

[1] Ruđer Bošković Institute, Division of Materials Physics, Laboratory for Molecular Physics and Synthesis of New Materials, and Centre of Excellence for Advanced Materials and Sensing Devices, Research Unit New Functional Materials, Bijenička c. 54, HR-10000 Zagreb, Croatia

ABSTRACT

Nanostructured materials play a significant role in numerous advanced and diversified applications many of which exploit their optical properties. Among these are nanostructured substrates for surface-enhanced Raman scattering (SERS). The objective of our study was to contribute to understanding of topological aspects influencing and underlying SERS on nanostructured substrates. To that purpose we fabricated Ag-decorated Si-nanowires (SiNWs) substrates with different fractal and lacunar characteristics. We demonstrated that fractal dimension and lacunarity have a profound influence on SERS enhancement. We discussed the involved interplay between long-range properties of nanostructured substrate, namely its fractal topology, and short-range local features on a nanometer scale related to the distribution of inter-wire gaps (i.e. lacunarity) which strongly affect the local field enhancement, altogether precipitating in significant increase of SERS. Explanation of a strong correlation found to exist between fractal dimension *D*, lacunarity and SERS enhancement and the observed abrupt increase of SERS at $D \approx 2.54$ are provided within the framework of the percolation theory. For a percolated fractal structure a strong enhancement depends on the excitation wavelength resonantly matching the heterogeneity sizes of inter nanowire gaps as characterized with a high lacunarity determining the distribution of localized optical excitations i.e. hot spots.

Keywords: *SERS, silicon nanowires, fractal nanostructure, lacunarity, SERS substrate,*

Introduction

Generally, optical properties of nanostructured materials play paramount role in numerous advanced and diversified applications. Among these is use of nanostructured substrates for Surface-Enhanced Raman Scattering (SERS) whose optical properties have profound influence on enhancement of Raman signal. SERS is a highly sensitive spectroscopic technique exploiting the effect of enhancement of weak Raman scattering by molecules adsorbed on nanostructured or rough metal surfaces. The exact mechanism of the enhancement effect of SERS is still a matter of debate in the literature. However, it is now generally agreed that the dominant contributor to SERS processes is the electromagnetic enhancement mechanism [1]. According to this model the inherently weak Raman signals, originating from molecules adsorbed on a substrate's surface are enhanced by several orders of magnitude if the molecules are localized in nanoscale regions of intense optical fields i.e. trapped between adjacent plasmonic surfaces in the substrate, so-called "hot-spots" [2]. Since the SERS signal intensity depends on analyte - plasmon interaction occurring after adsorption of the analyte molecules onto the SERS substrate, the SERS substrate plays a paramount role in the enhancement process. In that context, among the great variety of SERS substrates [3] the attention has recently turned towards fractal nanostructures due to their exceptional performances in SERS. Theoretically, such structures cannot support ordinary wave propagation due to their lack of translational invariance. Hence, plasmonic waves become localized within fractals. Since the long-range interactions are suppressed, the individual dipolar modes of metallic particles, being spatially localized, enhance the field within these nanoscopic substrate regions resulting in exceptional SERS enhancement [4, 5].

Recently, the use of silicon nanostructures, particularly silicon nanowires (SiNWs) as SERS substrates draw considerable attention [6-9]. This interest is motivated by high enhancement factors, large surface-to-volume ratios, high measurement reproducibility and relatively low-cost fabrication compatible with the well-established silicon technology. In regard to investigations of SiNWs structures, these were mostly limited to 2d arrays of vertically oriented wires, while less attention has been devoted to the investigation of random 3d structures [10-17].

As far as our knowledge goes so far there was no systematic inquiry into the relationship between characteristics of random fractal structures, namely values of fractal dimension and lacunarity, and its optical properties, particularly the enhancement of Raman scattering.

Furthermore, it is well known that percolation, a second order phase transition often results in dramatic changes in structure's properties. Hence, we expect that percolation occurring in nanostructures such as random silicon nanowires structure should have a profound influence on its optical properties, particularly regarding SERS, since the theory predicts that "hot spots" are much stronger at percolation thresholds [18]**.** However, so far this aspect has not been given sufficient attention.

In this context, our aim was to investigate the relation between fractal substrate structure, characterized by its fractal dimension and lacunarity, and Raman light scattering enhancement in relation to percolation. To that purpose we have used a substrate consisting of 3d randomly oriented SiNWs decorated with silver nanoparticles.

We demonstrate that on the one hand the strong Raman enhancement is strictly correlated with the substrate's fractal dimension, which in turn can be controlled with the synthesis temperature and, on the other hand, length scales at which the refractive index primarily fluctuates governed by structure's lacunarity. The observed results are explained within the framework of the percolation theory. Particularly we show that the abrupt change in SERS is result of a second order phase transition - percolation occurring in the nanostructure.

1. Methods

2.1. Nanowire synthesis and substrate fabrication

We synthetized samples of randomly oriented SiNWs intended to be used as SERS substrates on p-type Si substrates (⟨100⟩ orientation, and 5–10 Ωcm resistivity) by a vapour – liquid – solid (VLS) growth method in a low – pressure chemical vapour deposition (LPCVD) reactor using previously reported method [9]. Briefly, we first cleaned Si wafers applying standard cleaning procedures [19] followed by the thin pre-layer Au sputtering in Polaron E5000 sputter coater. Next, prior to application of the VLS method, we performed annealing for one hour at temperatures from 480°-560°C. The VLS process was carried out with 26% SiH_4 diluted in Ar at 270 sccm flow rate during 1h deposition period. In each experiment, the annealing temperature was the same as VLS deposition temperature. We decorated the randomly orientated

SiNWs obtained in the previous step by Ag nanoparticles using the same sputtering system for several minutes under constant Ar flow.

2.2. SERS measurements

For SERS measurements, the 3x3 mm size substrate samples were immersed in ethanol solution of mercaptophenylboronic acid $C_6H_7BO_2S$ (4-MPBA) for several hours and subsequently dried.

The Raman spectroscopy measurements were performed on Jobin Yvon T64000 Raman spectrometer in micro-single configuration. The laser power at 532 nm on the sample with ~1μm spot size was ~1–2 mW. For all experiments, the 50x/0.75 objective was used. Exposition time was 20s for 1 scan. Mapping features: 100 points, 10 μm step, 1 scan/point, 10 s/sc.

2.3 Fractal analysis

Fractal and lacunarity analysis were performed on grey-scale SEM images using Fractal 3e [20], Frac-Lac, a plug-in for Image J [21] and Gwyddion [22] software.

There are several methods available for determination of fractal dimension [23] from the grey-scale images (pixel intensity values 0-255) which are used by different software. Our selection of the method for determination of fractal dimension was based on its appropriateness for the problem at hand and on comparative evaluation of performances, advantages and disadvantages of various methods, as discussed in the literatule [23, 24].

We used Fractal 3e software [20] that uses the Difference statistics (dynamic scaling) method [25]. The *Difference Statistics (Dynamic Scaling) method* suitable for grey scale images, relies on establishing the difference function $\Delta f(\varepsilon)$ as a function of spatial scale, as described in Refs. [23] and [25]:

$$\Delta f(\varepsilon) = \langle [f(x,y) - f(x_0,y_0]^2 \rangle^{1/2} \quad (1)$$

Here, $f(x_0,y_0)$ is the value of the considered function (representing height or intensity) at reference point and $f(x, y)$ is its value at a point at distance ε from the reference point. The

difference is averaged over spatial extent of the considered surface/image. If the considered function is the height *h* then the difference function $\Delta h(\varepsilon)$ is also known as *hight-hight* correlation function.

Now, for $\varepsilon \leq \xi$:

$$\Delta f(\varepsilon) \sim \varepsilon^{H} \tag{2}$$

Here, ξ is lateral correlation length and $H = d\text{-}D$ is Hurst or Hölder exponent related to the embedding and fractal dimensions *d* and *D*, respectively [26-29].

Hence, taking the logarithm of both sides of Eq. 2 and letting ε to go to zero, the fractal dimension (in a three dimensional space) is obtained as [28]:

$$D = \lim_{\varepsilon \to 0} \left[3 - \frac{\log \Delta f(\varepsilon)}{\log \varepsilon} \right] \tag{3}$$

2.4. Lacunarity analysis

Lacunarity is generally inferred from patterns extracted from digital images using box counting method. The arrangement of pixels is examined using box-shaped elements from a set of arbitrary sizes, denoted ε. The box of size ε is placed successively over the entire image, and the number of pixels that fall within the box is recorded. Thus, from the pixel distribution in an image, obtained from scans at different box sizes and at different grid orientations (g) the lacunarity $\lambda(\varepsilon, g)$ is calculated as

$$\lambda(\varepsilon,g) = CV(\varepsilon,g)^2 = (\sigma/\mu)^2_{\varepsilon,g} \tag{4}$$

where *CV* is the coefficient of variation, σ and μ are standard deviation and mean for pixels per box at size ε, and orientation g [30,31]. Hence, there is a value of λ for each ε from each series of grid sizes and for each g, from a set of grid orientations.

The result is usually presented as a plot of Ln (λ) *vs*. Ln (ε).To avoid the computationally awkward situations that may occur with homogenous images with vanishing standard deviations and consequently undefined slopes of regression lines the results are transformed to

$$\Omega\lambda = \lambda + 1 = (\sigma/\mu)^2 + 1 \quad (5)$$

The slope of ln-ln regression line of λ over all ε is calculated for each *g* using this equation to avoid an "undefined" calculation. Namely, a completely homogeneous image will not vary in the pixels per box, so that the standard deviation, σ, for a box count at some ε will be 0. This means that $\lambda = (\sigma/\mu)^2 = 0$, which makes sense, but it also means that the ln of λ and therefore the slope of the ln-ln regression line for λ and ε would be undefined. Thus, we transform the data using λ+1, so that a completely homogeneous image has a slope of 0, corresponding intuitively to the idea of no rotational or translational invariance and no gaps [21].

2. Results and Discussion

3.1. Fabrication and characterization of the fractal SiNWs substrates

Fabrication of the nanostructured SiNWs SERS substrate requires synthesis of SiNWs mesh and decoration of nanowires with Ag nanoparticles as described in the Methods. We synthetized randomly oriented SiNWs substrates at different temperatures in the range 480°C - 560°C, resulting in different substrate structures. The structures of the SiNWs substrates were examined using Jeol JSM 7000F scanning electron microscope (SEM) under 10 kV. For further characterization of the substrates we performed fractal and lacunar analysis of grey scale SEM images. Representative SEM images of SiNWs substrates (recorded at the same magnification), as well as their three-dimensional views, generated by the Gwyddion software, are depicted in Fig. 1. SEM images reordered at an order of magnitude higher magnification reveal the SiNW coverage with Ag nanoparticles. After short sputtering times (3 and 5 min), the SiNWs are relatively uniformly decorated with oval Ag nanoparticles of 20–40 nm diameter (Fig. A.1 in the Appendices).

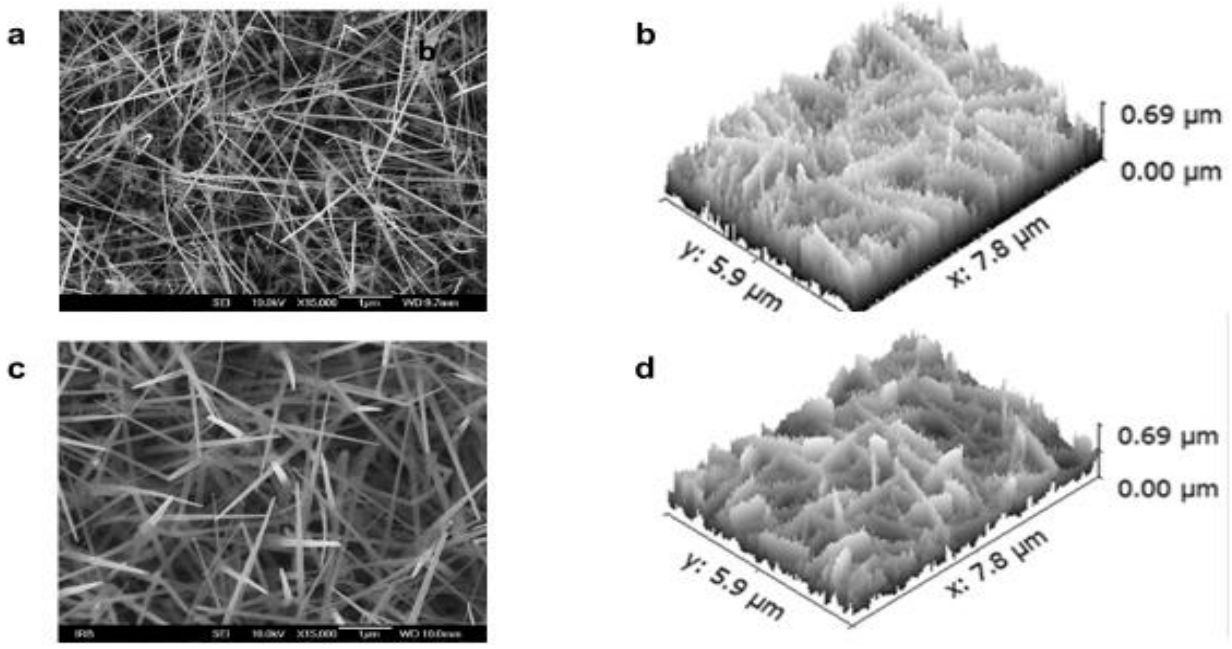

Fig. 1. SEM images and three dimensional views, of randomly oriented Si-nanowires SERS substrates. Substrates synthetized at T = 500 °C and at T = 560 °C are depicted in the upper (a-b) and lower (c-d) rows, respectively. The recorded SEM images (magnification 15000x), with dimensions 1280x1024 px, correspond to actual dimensions of 7.84 µm x 6.28 µm and height ≈ 0.7 µm (1px = 6.13nm).

In the SEM images similar yet distinctively different structures of SiNW substrates are clearly seen. The self - similarity of the substrate structures is revealed by inspecting SEM images taken at different magnifications (not shown here) and confirmed with subsequent fractal analysis. Analysis of the SEM images shows that the processing/synthesis temperature has a profound influence on structure and characteristics of substrates of randomly oriented SiNWs mesh. It also influences dimensions of the nanowires, particularly the thickness that increases with the increase of temperature viz. 45 – 70 nm and 120-180 nm for 500 ^{0}C and 560 ^{0}C, respectively. The surface roughness parameters inferred from SEM images (not presented here) also vary considerably and are correlated with the synthesis temperature as well as with the fractal dimension. The latter in compliance with the previous finding that there exists a strong correlation between certain roughness parameters and corresponding fractal dimension [32].

Next, we performed fractal and lacunarity analysis of grey scale SEM images. Fractal dimension D, as a measure of geometric complexity, is suitable for quantitative assessment of structures that are difficult to describe using classical Euclidean measures, and whose morphology is represented in binary or grayscale digital images. On the other hand, lacunarity can quantify additional features of patterns such as translational or rotational invariance and more generally, heterogeneity of a fractal structure. Lacunarity, being a measure of spatial heterogeneity provides means that can distinguish between two objects that have the same D but are structurally different. Thus, it can be used to differentiate between SEM images that have similar fractal dimensions but different appearances.

Firstly, we performed fractal analysis as described in the Methods. The analysis of SEM images established the fractal character of all considered substrates as documented further on.

Values of fractal dimensions D_g of SiNWs substrates inferred from their grey-scale SEM images are depicted in Fig. 2. D_g (subscript "*g"* denotes that the fractal dimension was derived from grey scale images) corresponds to the volume structure of the substrate, hence $2 < D_g < 3$. A higher value of D_g indicates that the considered fractal structure has a higher space-filling capacity. Obviously, all considered SiNWs substrates are fractal structures yet with different fractal dimensions resulting from different fabrication temperatures. In respect to the substrate fabrication temperatures the highest fractal dimension occurs at $T = 500\ ^0$C, with the value of about 2.65 (Fig.2).

Furthermore, the SiNW SERS substrate is a complex random structure and it would not be unexpected that it could also exhibit multifractal properties. Our preliminary multifractal analysis of substrate samples (see the Appendix D.) shows low to moderate degrees of multifractality. The involved (multi/bi) fractal dimensions do not differ much from corresponding D_g which represents the average value over all scales involved. The most important result of the preliminary fractal analysis is that there is no correlation between the degree of multifractality of our samples and the corresponding enhancement factors (the corresponding regression coefficient $R^2 = 0.1242$). Thus, further multifractal analysis is beyond the scope of this paper.

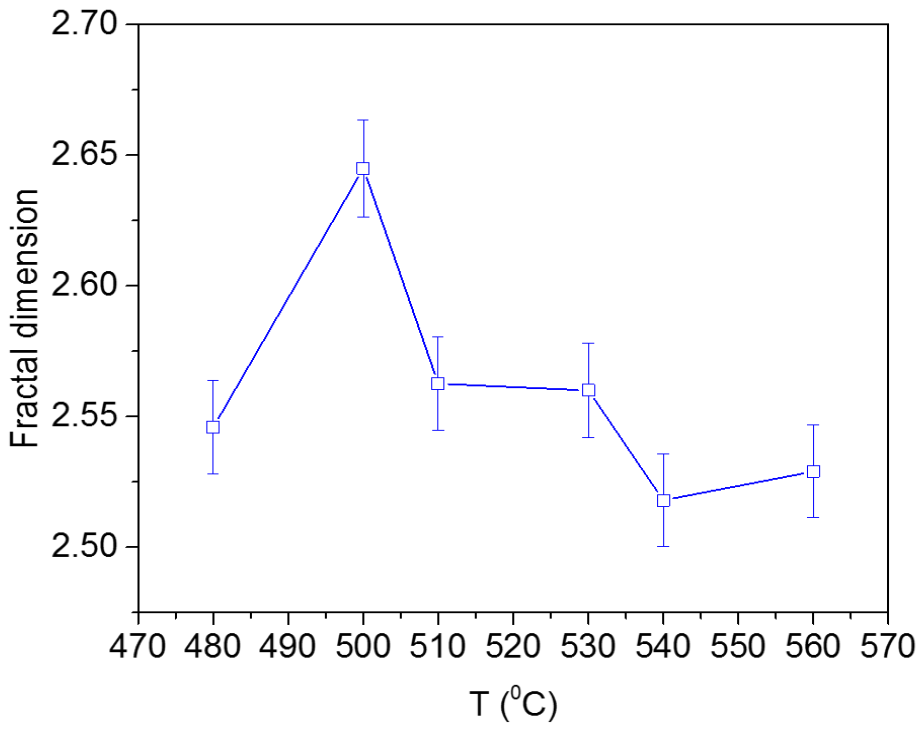

Fig. 2. Fractal dimensions of SiNWs substrates *vs*. fabrication temperature. Fractal dimensions of the substrates (identified by the fabrication temperature) were inferred from the corresponding grey-scale SEM images. The symbols represent average values and the error bars represent the corresponding standard deviations.

In light of the fact that the structures with lack of translational invariance prevent usual wave propagation and promote plasmonic wave localization within fractals resulting in exceptional SERS enhancement the lacunarity analysis of synthetized substrates is of high relevance for our study. Lacunarity is a concept distinct and independent from the fractal dimension and needs more than one numerical variable to be fully determined. Lacunarity is strongly related to the size distribution of the "holes" (voids) on the fractal structure and to its deviation from translational invariance. At a given scale, low lacunarity indicates homogeneous and transitionally invariant structure because all gap/voids sizes are of similar size, whereas objects of high lacunarity are heterogeneous and not transitionally invariant. However, it is important to note that high-lacunarity objects which are heterogeneous at small scales can be quite homogeneous at larger scales or vice versa. In other words, lacunarity is a scale-dependent measure of the spatial complexity of patterns [33, 34]. Hence, as a scale-dependent quantity the

lacunarity is usually presented as a lacunarity curve representing values of lacunarity *vs.* sampling window size (c.f. Fig. 3a). We determined the substrates' lacunarities from the corresponding SEM images following the procedure outlined in the Methods. The representative results of lacunarity analysis of grey-scale SEM images are presented in Fig. 3a, where the plot of average lacunarity $\Omega\lambda$ of grey-scale SEM images *vs.* window sampling element size is depicted.

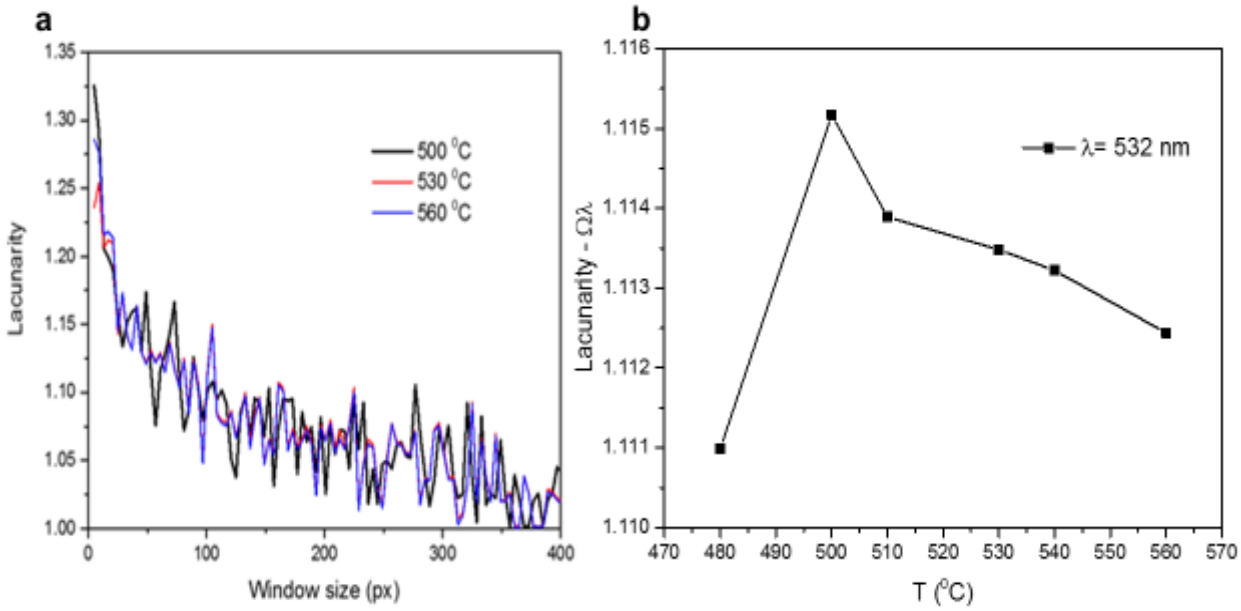

Fig. 3. Lacunarity of SiNWs SERS substrates. (**a)** Representative lacunarity curves of SiNWs substrates (identified with the fabrication temperature) *vs.* sampling window size (in pixels). Note that 1px = 6.13nm. (**b)** Average substrate lacunarity inferred from grey scale SEM images at sampling window sizes corresponding to the incident wavelength (532 nm) *vs.* substrate fabrication temperature.

Inspection of lacunarity curves depicted in Fig.3a shows that the lacunarity increases nearly exponentially with a decrease of the sampling window size and exhibits considerable fluctuations at greater sampling window sizes (> 50px). Since the lacunarity is a scale dependent quantity it is necessary to consider lacunarity at relevant scales i.e. these compatible with the involved wavelengths. Generally, strong light scattering occurs when the dimensions of a structural inhomogeneity are compatible with the effective wavelength of light propagating in the medium. The lacunarities of investigated substrates (identified by the fabrication temperature) at

sampling window sizes corresponding to the incident wavelength are depicted in Fig.3b. The maximum of lacunarity indicating relatively lower translational invariance of the substrate structure occurs for substrate manufactured at T = 500 ^{0}C with fractal dimension D_g = 2.65.

3.2. Analysis of enhancement of Raman scattering (SERS) in the fractal SiNWs substrates

We quantified the enhancement performances of fractal SiNWs substrates with SERS measurements performed on a Raman spectrometer in micro-single configuration with 532 nm excitation and using ethanol solution of mercaptophenylboronic acid (4-MPBA) as an analyte as described in the Methods.

The assemblies of nanostructures with fractal properties, whether ordered or disordered, profoundly influence the light transport inside the materials and, consequently, their optical properties, in particular the light scattering [1–5, 18]. When compared to non-fractal structures, where the surface plasmon modes are delocalized over a longer range, electromagnetic field enhancement in fractal structures due to the localization of plasmonic waves within fractals can be greater by an order of magnitude [35]. The localization occurs essentially by the confinement of local modes within the metal nanostructure, leading to a strong enhancement in the local plasmon intensity. In that context a “hot spot” is defined as a junction or close interaction of two or more plasmonic objects where at least one object has a small radius of curvature on the nm scale [36]. Hot spots are formed due to the collective and phase coherent excitation of localized surface plasmon resonance. The structural network of hot spots concentrates an incident electromagnetic field and effectively amplify the near field between and around the nanostructures. The intensity of surface-enhanced light scattering at a hot spot scales with the fourth power of the local field enhancement at the metal surface [37]. Moreover, the fractal geometry of such a system results in a scale-free localization, *i.e*. hot spots exist on all size scales ranging from those of the nanoscale components of the system to that of the entire structure. Also the size of the hot spots fluctuates widely across the structure. Altogether, in effect the overall enhancement should be structure dependent**.**

We have indeed observed such structure dependent enhancement of the spectral intensity as illustrated by SERS spectra of 10^{-3} M MPBA recorded at different fractal SiNWs substrates as depicted in Fig. 4. The 4-MPBA SERS spectral band assignment, not relevant for the present considerations, is given in the Ref. [38].

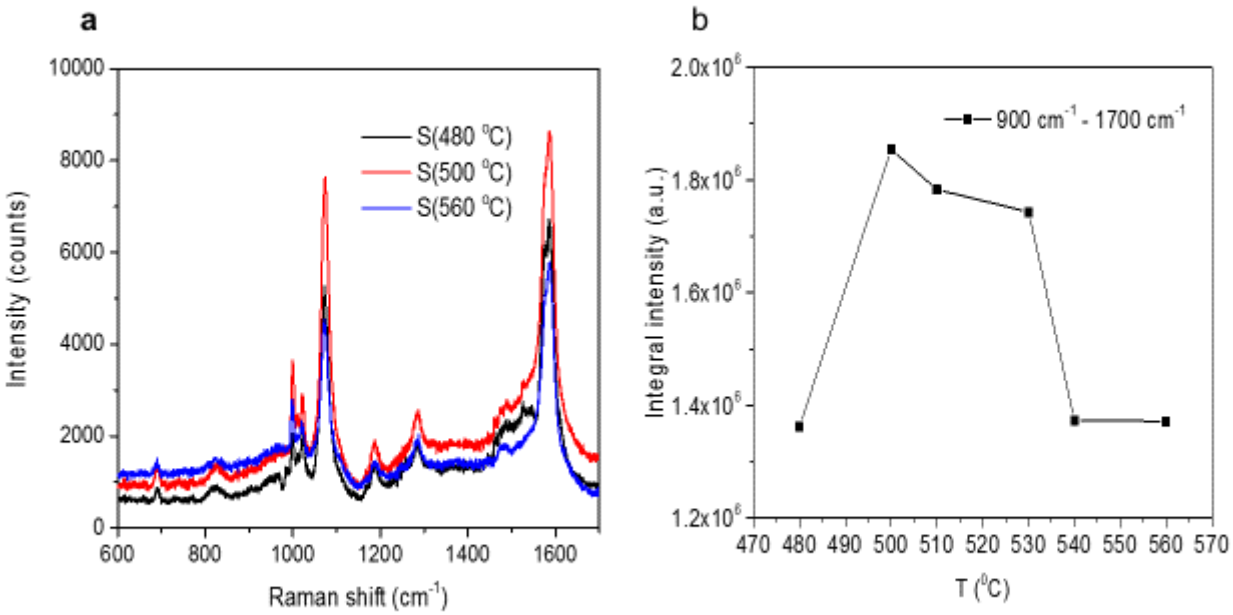

Fig. 4. Enhancement of SERS spectra. (**a)** Representative SERS spectra of 10^{-3} M MPBA recorded with the same experimental parameters at different SiNWs substrates *S(T)* designated by the corresponding fabrication temperature. (**b)** The integral intensity of 10^{-3} M MPBA Raman spectra in the relevant spectral range 900 cm^{-1} - 1700 cm^{-1} *vs*. the fabrication temperature of randomly oriented SiNWs mesh substrates.

From Fig. 4b, it can be clearly seen that the SERS intensity highly depends on substrate structure and that the highest integral SERS intensity is obtained using the substrate fabricated at *T*=500 ^{0}C. Such, substrate's structure dependent, intensity variation was also observed for single line intensities of principal Raman lines situated at ~ 1074 cm^{-1} and ~ 1585 cm^{-1}. This indicates that the enhancement process is independent of the specific molecular vibration, represented by its characteristic Raman shift, but rather related to the substrate structure. The same behavior was observed regardless of the investigated analyte concentration. It is obvious that, with all other parameters being equal, the intensity of Raman scattering depends on substrate structure which is

determined by the fabrication temperature and characterized by its fractal dimension and lacunarity. Mapping of the substrates responses (Fig. 2SI in the ESI) reveals relatively homogenous SERS response over the substrate surface with relative standard deviation SD ≤ 10%. It is commonly accepted that SD values around 20% indicate a fair grade of homogeneity in SERS detection [39, 40].

Next we discuss the interplay between long-range properties of nanostructured substrate, namely the fractal topology of the structure and the percolation phase transition, and short-range local features on the nanometer scale which are related to the distribution of inter particle/wire gaps (lacunarity) and strongly affect the local field enhancement. First, we examined the correlation between fractal dimensions of substrates D_g and corresponding spectral intensity enhancement. The dependence of integral SERS intensities on D_g for the relevant spectral band as well as the two main spectral lines cantered at ~ 1074 cm^{-1} and ~ 1585 cm^{-1} (cf. Fig. 4a) is depicted in Fig. 5a. The observed SERS intensities are well correlated with fractal dimension. The corresponding regression coefficients are 0.817, 0.879 and 0.855, respectively.

The enhancement factor (EF) calculated from SERS spectra for 10^{-3} M MPBA sample on the SiNWs substrates *vs*. corresponding fractal dimension is presented in Fig. 5b. The EF were calculated for Raman peak at ~1585 cm^{-1} (calculation details are described in ESI), and the enhancement is uniform over the whole surface, with a standard deviation of about 10%, as documented by mapping data presented in the ESI.

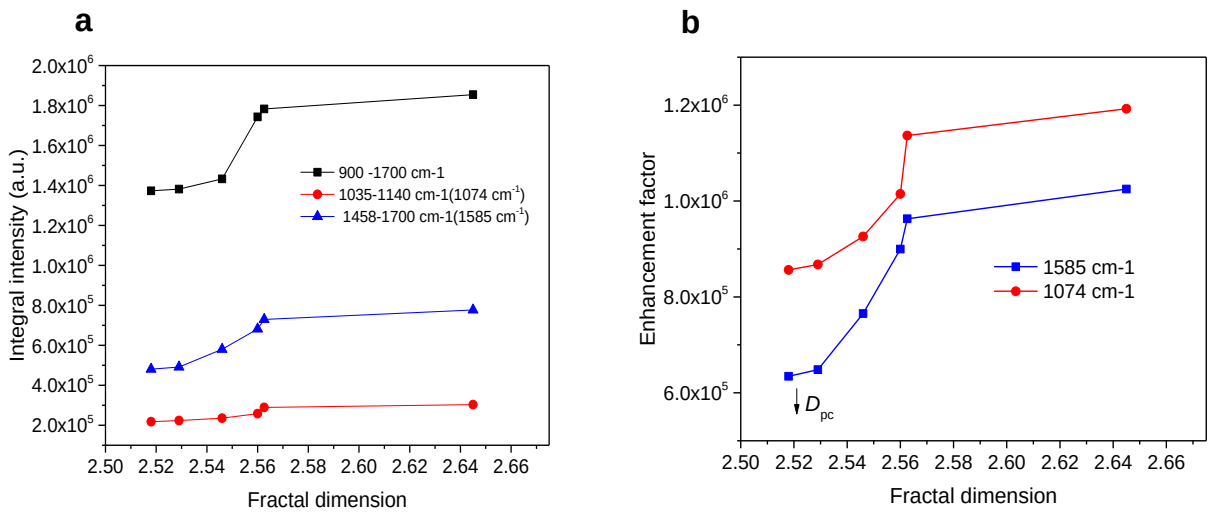

Fig. 5. Influence of substrate fractal dimension on Raman spectrum enhancement. (**a)** Integral Raman spectral band and line intensities of 10^{-3} M MPBA sample recorded at various substrates characterized with the corresponding fractal dimensions D_g. (**b)** Enhancement factor for principal SERS line at 1585 cm^{-1} *vs.* substrate's fractal dimension. D_{pc} denotes theoretical fractal dimension at the percolation threshold.

Inspection of plots of SERS intensity and enhancement factors *vs*. D_g (Fig. 5a and 5b) shows a threshold in the variation of the integral spectral intensities and a threshold in the corresponding EF occurring at about $D_g \approx 2.53$. After the threshold, SERS intensity and EF increase rapidly. For principal SERS line at 1585 cm^{-1} this rapid growth is confined to a narrow range of $2.54 < D_g < 2.56$ after the threshold value. In this range, a slight increase of D_g of only ~1% results in nearly doubling of enhancement factor. For $D_g > 2.57$ the spectral intensities and EF only slowly increase with a further increase of D_g.

The experimental data depicted in Fig.5, i.e. change of intensity/enhancement factor with change in fractal dimension, are excellently fitted with a sigmoidal-logistic growth model as illustrated in Fig. 6. Previously various sigmoidal growth models were extensively used in numerous studies of percolation such as e.g. investigation of the percolation threshold of electrical conductivity in polymer composites [41].

In our case the corresponding equation of a sigmoidal-logistic growth is given by:

$$Y = Y_0 + \frac{Y_m - Y_0}{1+(\frac{D}{D_0})^n} \quad (6)$$

Here, Y is the dependent variable (intensity, enhancement factor etc.), Y_0 is an initial/base value, Y_m is final value, D is fractal dimension, D_0 is point of maximal growth rate and n a slope factor.

Analysis of all fitted data, such as those depicted in Fig. 6 shows that the point of maximal growth rate D_0 of dependent variables (intensities and/or enhancement factors) is practically identical with value $D_0 = 2.555 \pm 0.003$, while the growth is confined to a very narrow D range. The values at 20% and 80% of corresponding maximal values $Y(20)$ and $Y(80)$ occur at $D = 2.546 \pm 0.005$ and $D = 2.563 \pm 0.003$. In application of sigmoidal-logistic growth to percolation problems it is often assumed that that the point of maximal growth rate (here D_0) corresponds to the percolation threshold [41].

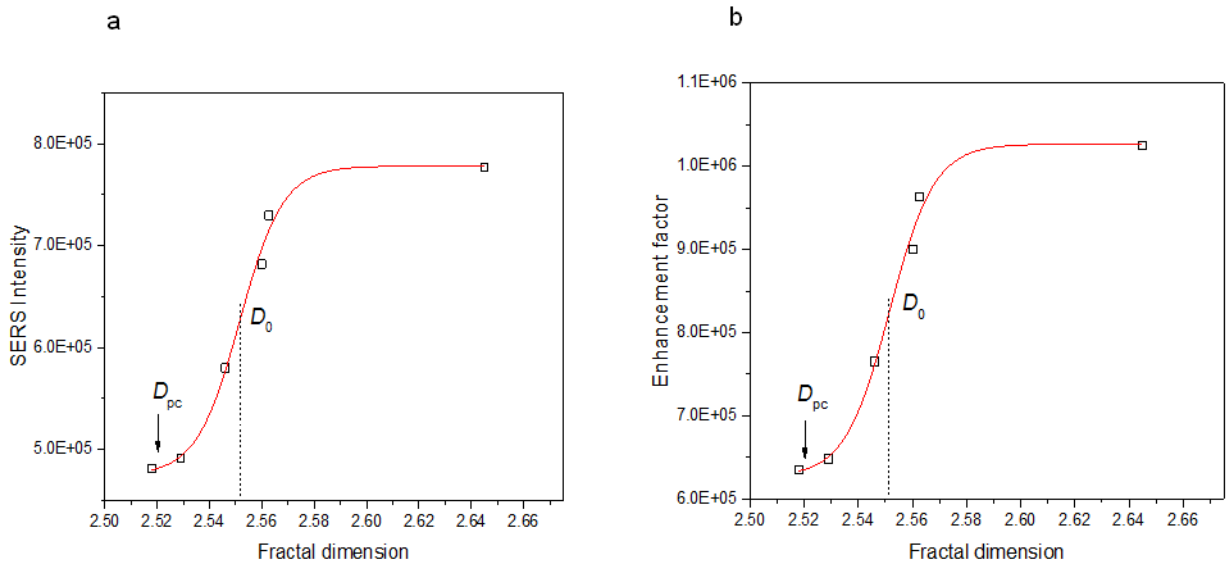

Fig. 6. **Fit of experimental data for principal SERS line at 1585 cm^{-1} *vs.* substrate's fractal dimension with sigmoidal-logistic growth model**. **(a)** SERS intensity and **(b**) the corresponding enhancement factor. Symbols denote experimental data and lines fit with the sigmoidal-logistic growth model**.** D_{pc} denotes theoretical fractal dimension at the percolation threshold and D_0 is point of maximal growth rate. $D_0 = 2.552$ and $R^2 = 0.9845$

Such experimentally observed behavior can be explained within the framework of the percolation theory [42]. Namely, the value of fractal dimension at the observed threshold of intensity/enhancement factor jump closely (within measurement uncertainty) corresponds to the theoretical percolation threshold in three dimensions (D_{pc} = 2.52) thus, indicating appearance of a connected, weakly correlated disordered structure [43]. Percolation, a second order phase transition, represents the basic model for a structurally disordered system. The percolation theory deals with development and growth of connectivity within structures, particularly aggregates and clusters. Percolation threshold is a mathematical concept in percolation theory, indicating the occurrence of a long-range connectivity in random systems. It is the critical value p_c of the occupation probability p, at which large structures/clusters and long-range connectivity first appears. Theoretically, when p approaches the critical point nanowire clusters grow and merge together to form an infinite connected cluster. The fractal dimension D_{pc} of a percolating system depends only on (Euclidian) dimensionality d of the system and not on details of local structure geometry [40]. The theoretical fractal dimensions at percolation thresholds for systems in three and two dimensions are 2.52 and 1.89, respectively.

Here, it is worth noting that the generated percolation structure dramatically modifies characteristics of the material: a structural phase transition occurs, the correlation length jumps, order parameter and the object symmetry and other parameters are changing, thus leading to changes in physical-chemical and mechanical characteristics. Such structures substantially modify the diffusion and conductivity processes, affect the kinetics of chemical reactions, define the mechanical strength and corrosion resistance, and lead to other phenomena [44-46]. Hence, we may conclude that in our case the significant increase of SERS occurs after the onset of percolation which results in a connected, weakly correlated structure. This is in line with theoretical prediction that the „hot spots" are much stronger at percolation threshold [47] and recent finding that for the gold films the maximum SERS signal was observed near the percolation threshold [48].

The structures with fractal dimensions below the percolation thresholds are not fully connected in a sense that they do not span the considered space. The crossing of the nanowires in the percolated SiNWs network leads to coupled plasmon behavior that spatially extends to encompass the regions between and significantly beyond the wires [49]. This strong coupling,

and porous percolated structure allowing more molecules to enter this high electric field regions result in a significant enhancement of the SERS effect and sensitivity.

The next relevant feature of the substrate's structure influencing the light enhancement is its lacunarity. Generally, strong light scattering occurs when the dimensions of a structural inhomogeneity are compatible with the effective wavelength of light propagating in the medium. Since the lacunarity is a scale dependent quantity it is necessary to consider lacunarity at relevant scales i.e. these compatible with the involved wavelengths. Since in our Raman measurements the laser wavelength is 532 nm the relevant scale – window size at which interaction takes place, i.e. lacunarity corresponding to inhomogeneity which laser "sees" is 532 nm.
Although the differences in lacunarity between the considered substrates are not very high their influence on the enhancement of the scattered intensity is significant. Since the relation between lacunarity and fractal dimension is a non-linear one (cf. Fig.8) the influence of lacunarity on signal enhancement is more complex. Consequently the behavior of enhancement factor with variation of lacunarity is somewhat different in comparison to the variation with corresponding fractal dimension. This is clearly seen from plots of the SERS intensities *vs*. lacunarity at the excitation wavelength presented in Fig. 6. For the excitation wavelength (532 nm) the SERS intensity *vs*. lacunarity exhibits similar behavior as observed in intensity vs. D_g plots (c.f. Fig. 5a), namely occurrence of intensity jump at samples with lacunarity $\Omega\lambda \approx 1.113$ ($D \approx D_{pc}$) and maximum for substrate with the highest lacunarity fabricated at 500^0C ($D = 2.65$). The correlation coefficients between lacunarity at excitation wavelength and the integral intensities of SERS spectral band and lines depicted in Fig. 7 are relatively high, with values 0.769, 0.745 and 0.668, respectively.

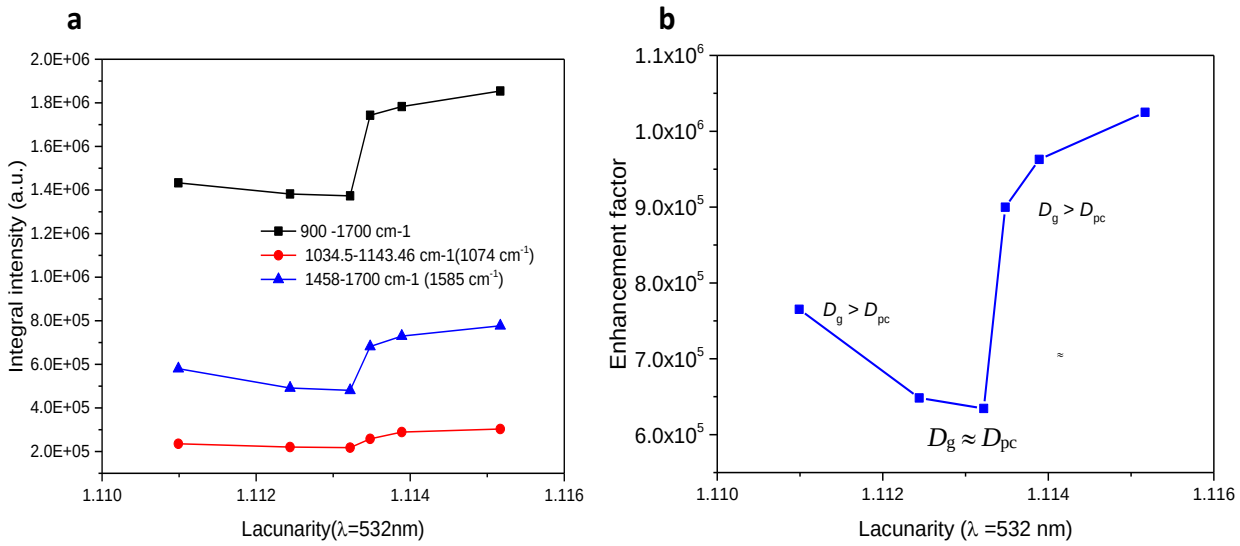

Fig. 7. Influence of substrate lacunarity at the excitation wavelength on Raman spectrum enhancement. (**a)** Integral Raman spectral band and line intensities of 10^{-3} M MPBA sample recorded at various substrates characterized with the corresponding lacunarity at the excitation wavelength (532 nm). (**b)** The enhancement factor for principal SERS line at 1585 cm^{-1} *vs.* substrate's lacunarity. The relative values of corresponding fractal dimensions D_g in respect to the value of fractal dimension at the percolation threshold D_{pc} are shown along the respective measurement points.

On the other hand, as expected theoretically lacunarity and fractal dimension are not correlated (c.f. Fig. 8), since, as mentioned before, lacunarities of structures with the same fractal dimension can be significantly different (or vice versa). Hence, we are dealing with two relatively independent parameters governing the enhancement of scattered intensity. Consequently this is manifested as a difference in respective regression coefficients as documented above. Now, in order to get a deeper insight into the intricate interplay between substrate's fractal dimension and lacunarity resulting in significant surface enhanced Raman scattering in Fig. 8 we put together all relevant information regarding the fractal dimensions, lacunarities and the SERS intensities.

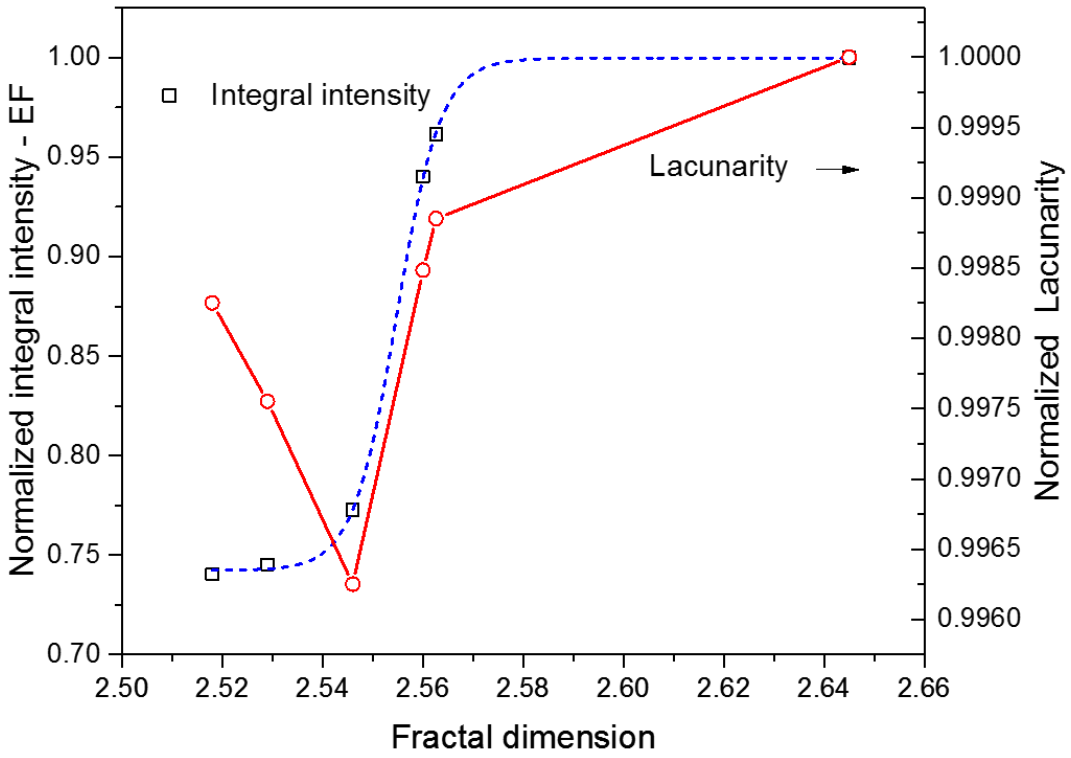

Fig. 8. Influence of substrate's fractal and lacunar characteristics on enhancement of Raman intensity. Normalized integral intensity (and EF) of considered SERS spectral band (900 cm^{-1} - 1700 cm^{-1}) of 10^{-3} M MPBA samples and normalized lacunarity corresponding to excitation wavelength *vs*. substrate's fractal dimension. *Note*: the values of normalized EF are identical to normalized intensity values. Symbols represent measurement points and dashed line a sigmoidal fit of normalized intensity (EF), D_0 = 2.554, D (10%) = 2.545.

Inspecting the plots in Fig. 8 we can see, aside from afore discussed change of enhancement with D, also a considerable dynamics and distinctive change of lacunarity with increase in fractal dimension. Initially as D_g increases the lacunarity decreases due to increase of connectivity of nanowires and increased size of connected clusters resulting in narrowing the size distribution of voids, i.e. the lacunarity. At the percolation threshold restructuring (a geometrical phase transition) occurs resulting in full connectivity and relative minimum of lacunarity ("neutral lacunarity"), compliant with theoretical predictions [50, 51]. Subsequent increase of lacunarity within the structure leads, due to decrease/lack of translational invariance, to enhanced scattering.

Thus, relatively high lacunarity per se does not result in significant enhancement of the scattering. Rather a fully percolated structure together with relatively high lacunarity is required for a significant increase of SERS and high enhancement factors. Furthermore, since the lacunarity is a scale dependent quantity it is different for different probing/excitation light wavelengths. Hence a corresponding pattern/distribution of localized optical excitations *i.e.* hot spots spatial positions will be strong function of the wavelength. This effect was indeed observed previously although it was not related to lacunarity [52].

3. Conclusions

We have investigated the influence of fractal and lacunar structural properties of randomly oriented Si-nanowires substrate on the enhancement of SERS. To that purpose we have synthetized SERS substrates with different fractal/lacunar structures using VLS approach. We discussed the involved interplay between long-range properties of nanostructured substrate, namely its fractal topology, and short-range local features on a nanometer scale related to the distribution of inter-wire gaps (i.e. lacunarity) which strongly affect the local field enhancement, altogether precipitating in significant increase of SERS. The results of our investigation have shown that:

- Fractal dimension and lacunarity of nanostructured SERS substrates have a profound influence on SERS enhancement.
- There exists a strong correlation between the enhancement of Raman scattering intensity and the corresponding fractal dimension and lacunarity of the considered substrate. No correlation between the degree of multifractality and the enhancement factor has been found.
- The observed correlations are explained within the framework of the percolation theory. Namely, we have shown that the observed abrupt increase in SERS occurring in SiNW structure with $D > D_{pc}$ is result of a second order phase transition – percolation;

- The occurrence of percolation, identified with corresponding fractal dimension D_{pc}, results in jump of enhancement factor. Thus, percolated nanostructured substrates exhibit high SERS response;

- Other parameter significantly influencing enhancement is lacunarity which is related to the size distribution of inter nanowire gaps and consequently influences distribution of localized optical excitations *i.e.* "hot spots" spatial positions

- The highest Raman scattering enhancement was obtained for a substrate with percolated structure lacking the translational invariance as indicated by a high lacunarity.

- Furthermore, for a percolated structure a strongly enhanced Raman emission, due to multiple scattering processes, is shown to depend on the excitation wavelength resonantly matching the heterogeneity sizes of the SiNWs fractal arrangement characterized with high lacunarity.
- The highest enhancement of Raman scattering intensity was observed for SiNWs substrate fabricated at 500 ^{0}C with D_g = 2.65 and lacunarity $\Omega\lambda$ = 1.115 at the excitation wavelength (532 nm).

As the enhancement of Raman scattering depends on fractal and lacunar characteristics of the substrate that are in turn determined by synthesis/annealing temperature, the selection of the processing temperature allows the design of a substrate with optimal performances. The observed performances make this novel random fractal architecture of SiNW-mesh very promising and reliable substrate for SERS. Altogether, the results of this study represent significant advancement in understanding of influence of fractal and lacunar features of a nanostructured substrates on SERS.

Corresponding Authors

* E-mail: Dubravko.Risovic@irb.hr

* E-mail: Hrvoje.Gebavi@irb.hr

Acknowledgements

This work has been supported by SAFU, project KK.01.1.1.01.0001 and by Croatian Science Foundation under the project (IP-2014-09-7046).

REFERENCES

[1] P.L. Stiles *et al.* Surface-enhanced Raman spectroscopy, Annu. Rev. Anal. Chem, 1 (2008**)** 601-626. https://doi.org/10.1146/annurev.anchem.1.031207.112814

[2] E. Le Ru and P. Etchegoin Eds., Principles of Surface-Enhanced Raman Spectroscopy: and related plasmonic effects, Elsevier Science: Oxford, 2008. ISBN**:** 9780444527790

[3] P.A. Mosier-Boss, Review of SERS Substrates for Chemical Sensing. Nanomaterials, *7* (2017**)** 142. https://doi.org/10.3390/nano7060142

[4] M.I. Stockman., V.M. Shalaev, M. Moskovits, R. Botet and T.F. George, Enhanced Raman scattering by fractal clusters: Scale-invariant theory, Phys. Rev. B 46 **(**1992) 2821–2831. https://doi.org/10.1103/PhysRevB.46.2821

[5] A. V. Markel, M. V. Shalaev, B. E. Stechel, W. Kim and L. R. Armstrong, Small-particle composites. I. Linear optical properties, Phys. Rev. B, 53 (1996) 2425–2436. https://doi.org/10.1103/PhysRevB.53.2425

[6] L. Mikac *et al*., Metal Nanoparticles Deposited on Porous Silicon Templates as Novel Substrates for SERS, Croat. Chem. Acta. 88 (2015) 437–444. https://doi.org/10.5562/cca2769

[7] X. Sun, L. Lin, Z. Li, Z. Zhang and J. Feng, Fabrication of silver-coated silicon nanowire arrays for surface-enhanced Raman scattering by galvanic displacement processes, Appl. Surf. Sci. 256 (2009), 916-920. https://doi.org/10.1016/j.apsusc.2009.08.085

[8] H. Gebavi *et al*., Silicon Nanowires Substrates Fabrication for Ultra-Sensitive Surface Enhanced Raman Spectroscopy Sensors, Croat. Chem. Acta, 90(2) (2017) 259–262. https://doi.org/10.5562/cca3127

[9] H. Gebavi *et al.*, Horizontal silicon nanowires for surface-enhanced Raman spectroscopy, Mater. Res. Express 5 (2018) 015015. https://doi.org/10.1088/2053-1591/aaa152

[10] B. Fan *et al.*, Silicon nanowire arrays coated with electroless Ag for increased surface-enhanced Raman scattering, Appl. Materials 3 (2015) 056101. https://doi.org/10.1063/1.4921040

[11] V. S. Vendamani *et al*., Three-dimensional hybrid silicon nanostructures for surface enhanced Raman spectroscopy based molecular detection, J. Appl. Phys. 23 (2018) 014301. https://doi.org/10.1063/1.5000994

[12] J. Yang, J. B. Li, Q. H. Gong. J. H. Teng and M. H. Hong, High aspect ratio SiNW arrays with Ag nanoparticles decoration for strong SERS detection, Nanotechnology 25 (2014) 465707. https://doi.org/10.1088/0957-4484/25/46/465707

[13] A. Convertino and M. Luca, Disordered array of Au covered Silicon nanowires for SERS biosensing combined with electrochemical detection, Scientific Reports 6 (2016) 25099. https://doi.org/10.1038/srep25099

[14] M. L. Zhang *et al.*, High-Efficiency Surface-Enhanced Raman Scattering Substrate Based Silicon Nanowires Array Decorated with Silver Nanoparticles, J. Phys. Chem. C 114 (2010) 1969–1975. https://doi.org/10.1021/jp902775t

[15] M. S. Schmidt, J. Hübner and A. Boisen, A. Large Area Fabrication of Leaning Silicon Nanopillars for Surface Enhanced Raman Spectroscopy, Adv. Opt. Mater. 24 (2012) OP11–OP18. https://doi.org/10.1002/adma.201290051

[16] X.Yang, H. Zhong, Y. Zhu, J. Shen and C. Li, Ultrasensitive and recyclable SERS substrate based on Au-decorated Si nanowire arrays, Dalton Trans. 42 (2013) 14324–30. https://doi.org/10.1039/C3DT51686E

[17] E. Cara, L. Mandrile *et al.*, Influence of the long-range ordering of gold-coated Si nanowires on SERS, Scientific Reports 8 (2018) 11305. https://doi.org/10.1038/s41598-018-29641-x

[18] V. M. Shalaev and A. K. Sarychev, Nonlinear optics of random metal-dielectric films, Phys. Rev B, 57 (20), (1998), 13265-13288. https://doi.org/10.1103/PhysRevB.57.13265

[19] W. Kern, The Evolution of Silicon Wafer Cleaning Technology, J. Electrochem. Soc. 137(6) (1990) 1887-1892. https://doi.org/10.1149/1.2086825

[20] Fractal3e. (2011). Fractal analysis system for Windows –software download and documentation. Available online at: http://cse.naro.affrc.go.jp/sasaki/fractal/fractal-e.html (accessed March 2020).

[21] http://rsb.info.nih.gov/ij/plugins/fraclac/FLHelp/Introduction.htm (accessed Juni 2020). .

[22] http://gwyddion.net/ (accessed March 2020).

[23] D. Risović and Ž. Pavlović, Performance Assessment of Methods for Estimation of Fractal Dimension From Scanning Electron Microscope Images, Scanning 35 (2013) 402–411. https://doi.org/10.1002/sca.21081

[24] E. Hadzieva, *et al*. Review of the Software Packages for Estimation of the Fractal Dimension, in S. Loshkovska, S. Koceski (Editors): ICT Innovations 2015, Web Proceedings, ISSN 1857-7288 © ICT ACT http://ictinnovations.org/2015, 2015ICT

[25] A.P. Pentland, Fractal based description of natural scenes, IEEE Trans. Pattern Anal. Mech. Intell. 6 (1984) 661–674. https://doi.org/10.1109/TPAMI.1984.4767591

[26] M. Li J., Lu. Li, M.O. Lai and B. Ralph, Image-based fractal description of microstructures. Kluwer Academic Publishers: Boston 2003. ISBN 978-1-4020-7507-0

[27] B. Dubuc, S.W. Zucker., C.Tricot, J.F. Quiniou and D. Wehbi, Evaluating the fractal dimension of surfaces, Proc. R. Soc. London A 425 (1989) 113–127. https://doi.org/10.1098/rspa.1989.0101

[28] K. Falconer, Fractal geometry, mathematical foundations and applications. John Wiley and Sons, Inc.: Chichester, 1990. ISBN: 978-1-119-94239-9

[29] W.S. Chen, S.Y. Yuan and C.M. Hsieh, Two algorithms to estimate fractal dimension of gray-level images, Opt. Eng. 42 (2003) 2452–2464. https://doi.org/10.1117/1.1585061

[30] T.G. Smith Jr., G.D. Lange and W.B. Marks, Fractal methods and results in cellular morphology - dimensions, lacunarity and multifractals, Journal of Neuroscience Methods 28(2) (1996) 123-136. https://doi.org/10.1016/S0165-0270(96)00080-5

[31] R. E. Plotnick *et al*. Lacunarity analysis: A general technique for the analysis of spatial patterns, Phys. Rev. E 53 (1996) 5461-5468. https://doi.org/10.1103/PhysRevE.53.5461

[32] S. Mahović Poljaček, D. Risović, K. Furić and M. Gojo, Comparison of fractal and profilometric methods for surface topography characterization, Appl. Surf. Sci. 254 (2008) 3449–3458. https://doi.org/10.1016/j.apsusc.2007.11.040

[33] R. E. Plotnick, R. H. Gardner, and R. V. O'Neill, Lacunarity indices as measures of landscape texture, Landscape Ecology 8(3) (1993) 201-211. https://doi.org/10.1007/BF00125351

[34] Y. Quan, Y. Xu , Y. Sunand and Y. Luo, Lacunarity Analysis on Image Patterns for Texture Classification, IEEE Conference on Computer Vision and Pattern Recognition (2014) 160-167. https://doi.org/10.1109/CVPR.2014.28

[35] L. He, N.K. Kim, H. Li, Z. Hu, and M. Lin, Use of a Fractal-like Gold Nanostructure in Surface-Enhanced Raman Spectroscopy for detection of selected food contaminants, J. Agric. Food Chem. 56 (2008) 9843–9847. https://doi.org/10.1021/jf801969v

[36] S. L Kleinman, R. R. Frontiera, A.I. Henry, J. A.Dieringer, and R. P. Van Duyne, Creating, characterizing, and controlling chemistry with SERS hot spots. Phys. Chem. Chem. Phys., 15(1), (2013). 21–36. https://doi.org/10.1039/c2cp42598j

[37] P. Alonso-González, *et al*. Resolving the electromagnetic mechanism of surface-enhanced light scattering at single hot spots, *Nat. Commun.* **3,** 684 (2012) 1-7. https://doi.org/10.1038/ncomms1674

[38] Pham, X., Shim, S., Kim, T. *et al.*, Glucose Detection Using 4-mercaptophenyl Boronic Acid-incorporated Silver Nanoparticles-embedded Silica-coated Graphene Oxide as a SERS Substrate, Bio Chip J. 11(1) (2017) 46-56. https://doi.org/10.1007/s13206-016-1107-6

[39] X. Tang, W. Cai, L. Yang and J. Liu, Highly uniform and optical visualization of SERS substrate for pesticide analysis based on Au nanoparticles grafted on dendritic α-Fe_2O_3, Nanoscale, 5 **(**2013) 11193-11199 https://doi.org/10.1039/c3nr03671e

[40] J. Quan, J. Zhang, X. Qi, J. Li, N. Wang and Y.Zhu, A study on the correlation between the dewetting temperature of Ag film and SERS intensity, *Scientific Reports* 2017, **7**, *14771* https://doi.org/10.1038/s41598-017-15372-y

[41] M. Rahaman, A. Aldalbahi, P. Govindasami,N. P. Khanam, S. Bhandari, P. Feng and T. Altalhi, A New Insight in Determining the Percolation Threshold of Electrical Conductivity for Extrinsically Conducting Polymer Composites through Different Sigmoidal Models, Polymers 9 (2017**)** 527 https://doi.org/10.3390/polym9100527

[42] D. Stauffer and A. Aharony , Introduction to Percolation Theory; Taylor and Francis: London, 1992. https://doi.org/10.1201/9781315274386

[43] J. Zierenberg *et al.*, Percolation thresholds and fractal dimensions for square and cubic lattices with long-range correlated defects, Phys. Rev. E. 96 (2018) 062125. https://doi.org/10.1103/PhysRevE.96.062125

[44] A. Herega , Some Applications of the Percolation Theory: Brief Review of the Century Beginning, J. Mat. Sci. Engineering A. 5 (11-12), (2015) 409-414. https://doi.org/10.17265/2161-6213/2015.11-12.004

[45] P. Bonnet, D. Sireude, B. Garnier and O. Chauvet, Thermal properties and percolation in carbon nanotube-polymer composites, Appl. Phys. Lett. 91 (2007) 01910. https://doi.org/10.1063/1.2813625

[46] D. Risović, S. Frka and Z. Kozarac, The Structure of Percolating Lipid Monolayers, J. Coll. Interface Sci. 373 (2012) 116–121. https://doi.org/10.1016/j.jcis.2011.12.009

[47] Optical properties of nanostructured random media, Vladimir M. Shalaev Ed., Springer Verlag Berlin, Heidelberg 2002, ISSN 0303-4216, 454pp (p. 169) ISBN 3540449485,

[48] D. E. Tatarkin *et al*., Surface-Enhanced Raman Spectroscopy on Hybrid Graphene/Gold Substrates near the Percolation Threshold, Nanomaterials, 10 (2020) 164. https://doi.org/10.3390/nano10010164

[49] S. M. Prokes, O.J. Glembocki, R. Rendell and M. Ancona, Effect of crossing geometry on the plasmonic behavior of dielectric core/metal sheath nanowires, Appl. Phys. Lett. 90 (2007) 093105. https://doi.org/10.1063/1.3094129

[50] J.P. Hovi, A. Aharony, D. Stauffer, and B. B. Mandelbrot, Gap Independence and Lacunarity in Percolation Clusters**,** Phys. Rev. Letters, 77(5) (1996) 877-880 https://doi.org/10.1103/PhysRevLett.77.877

[51] B. B. Mandelbrot and D. Stauffer, Antipodal correlations and the texture (fractal lacunarity) in critical percolation clusters, J. Physics A 27(9) (1994). L237-L242. https://doi.org/10.1088/0305-4470/27/9/001

[52] S. Ducourtieux *et al*., Near-field optical studies of semicontinuous metal films, Phys. Rev. B, 64 (2001) 165403. https://doi.org/10.1103/PhysRevB.64.165403

APPENDICES

A. Decoration of SiNWs with Ag nano-particles

SiNWs were relatively uniformly decorated with Ag nanoparticles using Polaron E5000 sputter coater for several minutes under constant Ar flow. The representative SEM image of Ag-decorated SiNWs is presented in Fig. A.1

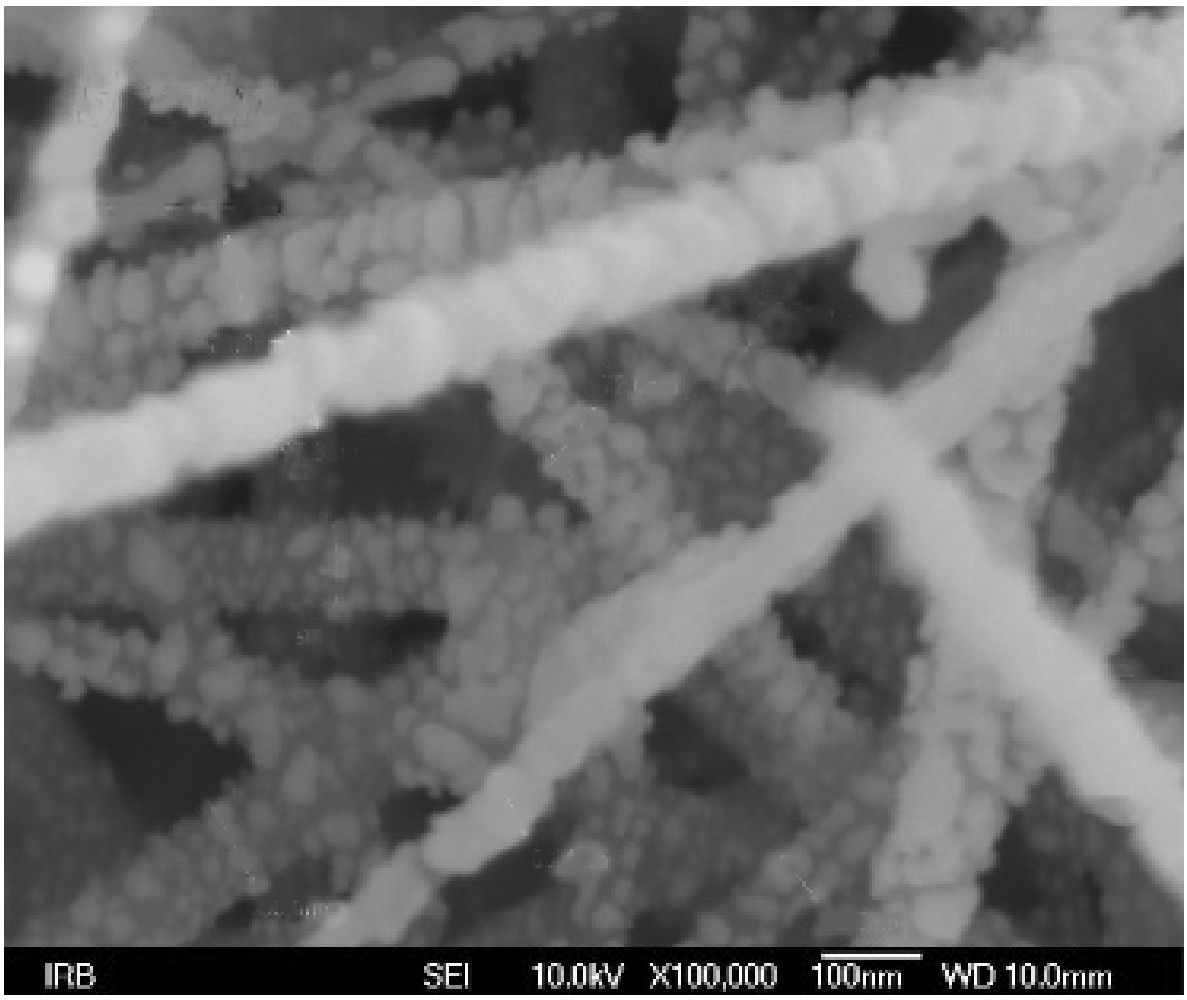

Fig. A.1 Ag-decorated SiNWs. Sputtering time 5 min. The approximate size of oval Ag nanoparticles is in the range of 20 – 30 nm

B. Raman mapping

The uniformity of SERS response over an active substrate is a crucial aspect in view of real applications. To evaluate it we mapped the SERS response across the representative substrate. The Raman spectroscopy measurements were performed on Jobin Yvon T64000 Raman spectrometer in micro-single configuration. The laser power at 532 nm on the sample with ~1μm spot size was ~1–2 mW. For all experiments, the 50x/0.75 objective was used. Exposition time was 20s for 1 scan.

The step size of the mapping was 10 μm, and one image contained the data from 100 scanning points. The SERS spectra of 100 points can integrate to generate artificial color images based on the intensity of a designated Raman peak. Results of mapping of 10^{-3} MPBA of 1073 cm^{-1} Raman band are presented in Fig. B.1

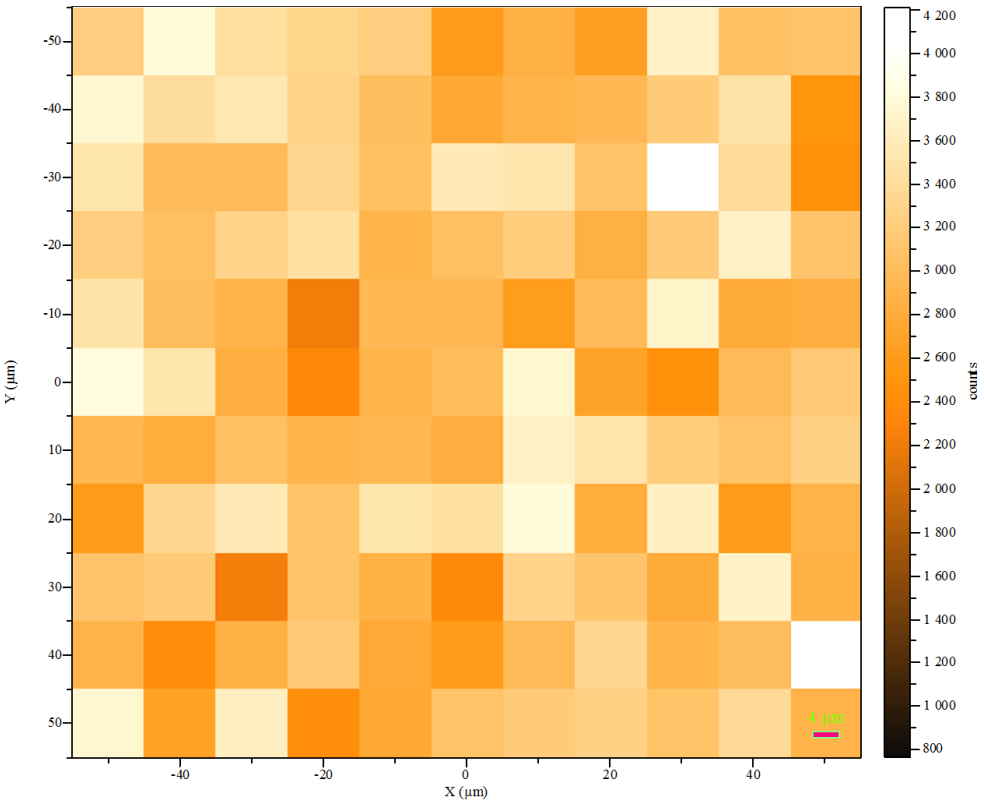

Fig. B.1. Mapping of 1073 cm^{-1} Raman band a 10^{-3} MPBA sample. Mapping features: 100 points, 10 μm step, 1 scan/point, 10 s/sc. Maximal intensity 4200 counts. Average intensity: 3420 ± 358 (≈ ± 10%) counts.

To assess the spatial homogeneity of a substrate the relative standard deviation (RSD) of signal obtained from multiple scanning is widely adopted in the SERS community [B.1, 2].

The average intensity inferred from substrate mapping using 10^{-3} MPBA and 1073 cm^{-1} Raman band is 3420 ± 358 counts. The corresponding RSD is $\approx$ 10%. This is a very good result since it is commonly accepted that RSD values around 20% indicate a fair grade of homogeneity in SERS detection [B.2-4].

References

[B.1] Fu, Q. *et al*. Highly Reproducible and Sensitive SERS Substrates with Ag Inter-Nanoparticle Gaps of 5 nm Fabricated by Ultrathin Aluminum Mask Technique. *ACS Appl. Mater. Interfaces* 7 (2015) 13322–13328, https://doi.org/10.1021/acsami.5b01524

[B.2] Peksa, V. *et al*. Testing gold nanostructures fabricated by hole-mask colloidal lithography as potential substrates for SERS sensors: sensitivity, signal variability, and the aspect of adsorbate deposition. *Phys. Chem. Chem. Phys.* 18 (2016) 19613–19620, https://doi.org/10.1039/C6CP02752K

[B.3] Wu, W. *et al*. Low-Cost, Disposable, Flexible and Highly Reproducible Screen Printed SERS Substrates for the Detection of Various Chemicals. *Sci. Rep.* 5 (2015) 10208, https://doi.org/10.1038/srep10208

[B.4] Luo, Z. *et al*. Net-like assembly of Au nanoparticles as a highly active substrate for surface-enhanced Raman and infrared spectroscopy. *J. Phys. Chem. A* 113 (2009) 2467–2472, https://doi.org/10.1021/jp810387w

C. Calculation of enhancement factor

SERS enhancement factor values were calculated from the average intensity of the appropriate MPBA spectral peak (~1585 cm^{-1}) measured in the three SERS experiments and corresponding peak of normal Raman measurements measured from a 1M aqueous solution of MPBA according to the method proposed in refs. [C.1-3]. Both SERS and Raman measurements were performed on Jobin Yvon T64000 Raman spectrometer in micro-single configuration under identical experimental conditions. The laser power@532 nm on the sample was ~1–2 mW. For all experiments, the 50x/0.75 objective was used. Exposition time was 20s for 1 scan.

The SERS enhancement factor (EF) is given by:

$$EF = \frac{I_{SERS}/N_{SERS}}{I_R/N_R} \quad \text{(C.1)}$$

where N_{SERS} and N_R represent the numbers of 4-MPBA molecules in the excitation volume measured using a SERS substrate and normal Raman, respectively. I_{SERS} and I_R are the signal intensities measured using SERS and normal Raman, respectively.

For SERS the excited volume was approximated as a cylinder with a base corresponding to the diameter of focused laser spot and a height corresponding to approximate focus depth of laser beam *Dof*.

The area of the focused laser spot S_{spot} can be calculated as

$$S_{spot} = \pi \frac{(1.22\lambda/NA)^2}{4}, \quad \text{(C.2)}$$

and the depth of focus is calculated from:

$$Dof = \frac{8\lambda}{\pi} NA^2 \quad \text{(C.3)}$$

where λ and *NA* are the laser wavelength and numerical aperture of the objective, respectively.

To measure the Raman intensity a drop (4μL) of 1M 4-MPBA was deposited on solid substrate, and then excited with a focused laser beam. The excitation volume was calculated from the laser spot size (Eq.C.2) and corresponding thickness of MPBA layer.

Then the number of the molecules was calculated using the excitation volumes and corresponding concentrations. Afterwards, using measured intensities the EF of the system can be easily calculated from (Eq.C.1). An enhancement factor of 1.02×10^6 was obtained for spectral peak at ~1585 cm^{-1}. This value is in the same order of magnitude of the one reported in ref. [C.2] on silver coated silicon nanopillars substrate.

References

[C.1] Le Ru, E. C., Meyer, M., Etchegoin, P. G., Le Ru, E. C. & Blackie, E. Surface Enhanced Raman Scattering Enhancement Factors: A Comprehensive Study. *J. Phys. Chem. C* 111 (2007) 13794–13803, https://doi.org/10.1021/jp0687908

[C.2] Schmidt, M. S., Hubner, J. & Boisen, A. Large area fabrication of leaning silicon nanopillars for Surface Enhanced Raman Spectroscopy. *Adv. Mater.* 24 (2012) 11–18, https://doi.org/10.1002/adma.201103496

[C.3] Hu, Y. S. *et al*. Enhanced Raman Scattering from Nanoparticle-Decorated Nanocone Substrates: A Practical Approach to Harness In-Plane Excitation. *ACS Nano* 4 (2010) 5721–5730 https://doi.org/10.1021/nn101352h

D. Multifractal analysis

The theoretical basis of multifractality can be found in the literature [D.1]; Block et al., 1990; Vicsek, 1992;Jestczemski and Sernetz, 1996] and is not covered here. Instead, we present a brief introduction necessary for understanding of results of our preliminary multifractal analysis.

For a homogeneous (monofractal) system, the probability (P) of a measure (here a number of pixels) appearing in a box varies with box size or scale L as

$$P(L) \sim L^{D} \tag{D.1}$$

where D is a fractal dimension. For heterogeneous (multifractal) systems, the probability within the ith region P_i scales as:

$$P_i(L) \sim L^{\alpha i} \tag{D.2}$$

where α_i is the Lipschitz-Holder exponent or singularity strength, characterizing scaling in the ith region.

The values of αi can be found at different positions within a distribution by the box counting technique. Then, the number of boxes $N(\alpha)$ where the P_i has singularity strengths between α and $\alpha + d\alpha$ is found to scale as [D.2]:

$$N(\alpha) \sim L^{-f(\alpha)} \tag{D.3}$$

Where $f(\alpha)$ can be defined as the fractal dimension of the set of boxes with singularities α.

$$\alpha(q) = \frac{\sum_{i=1}^{N_\tau} \mu_i \ln P_i}{\ln L}$$

$$f(\alpha) = \frac{\sum_{i=1}^{N_\tau} \mu_i \ln \mu_i}{\ln L} \quad \text{(D.4)}$$

μ = mean value of the probability distribution at some L

A homogeneous fractal exhibits a narrow $f(\alpha)$-spectrum, whereas the opposite is true for an heterogeneous fractal.

The spectrum width or degree of multifractality is defined as

$$\Delta f(\alpha) = \alpha_{max} - \alpha_{min}. \quad \text{(D.5)}$$

This is illustrated in Fig D.1 where representative $f(\alpha)$-spectra for samples with low and moderate multifractality are depicted. The corresponding degrees of multifractality $\Delta f(\alpha)$ for substrates 480^0C and 500^0C are 0.39 and 0.80, respectively.

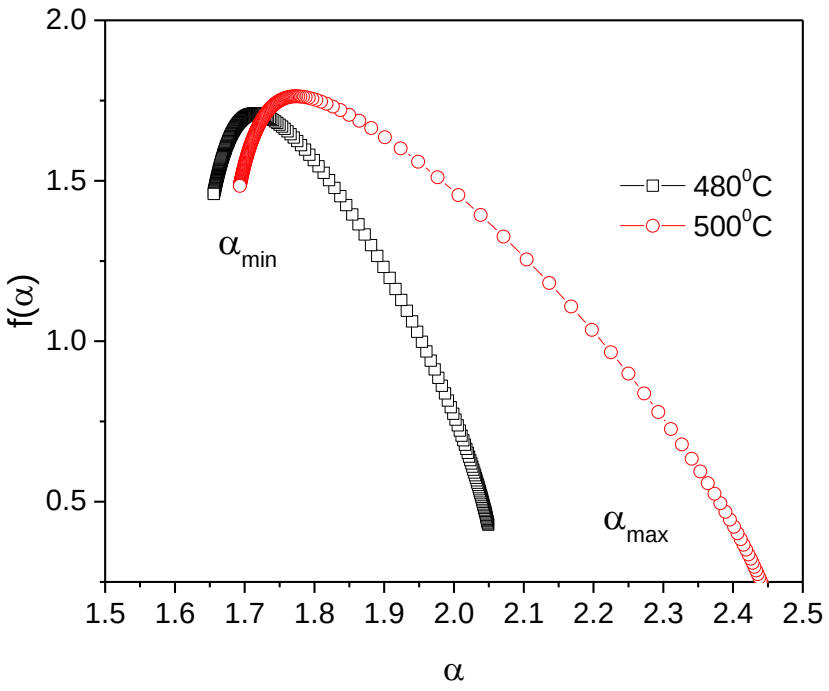

Fig. D.1 Multifractal spectrum for samples 480^0C and 500^0C with low and moderate multifractality, respectively. Respective degrees of multifractality $\Delta f(\alpha)$ are 0.39 and 0.80

Calculated degrees of multifractality for all investigated samples are depicted in Fig. D.2. The highest degree of multifractality (0.81) is obtained for substrate 500^0C, while other substrates exhibit significantly lower $\Delta f(\alpha)$ with average value 0.52 ± 0.1

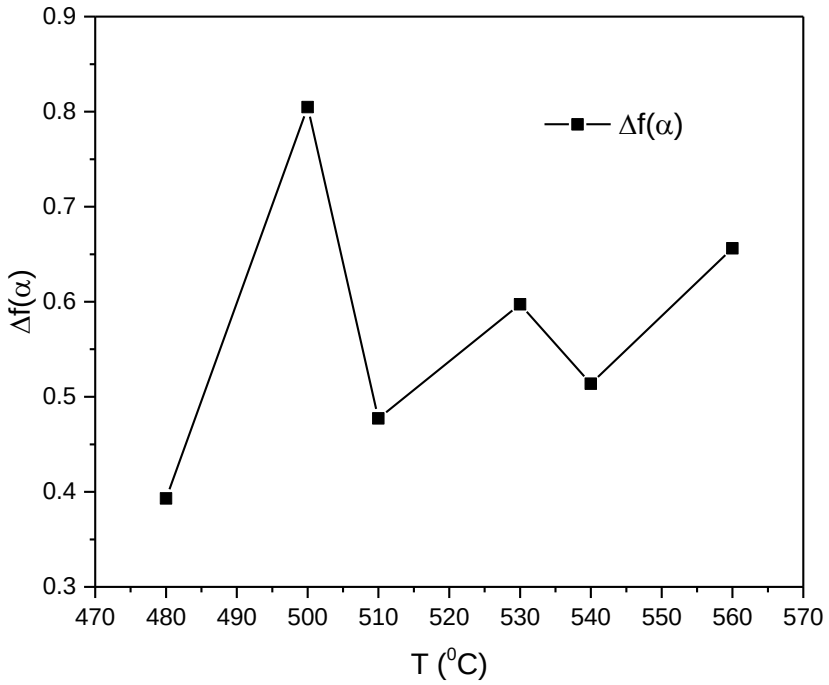

Fig. D. 2 Degrees of multifractality $\Delta f(\alpha)$ for all investigated samples identified with corresponding manufacturing temperature.

The most important result of our preliminary multifractal analysis is that there is no correlation between degree of multifractality of investigated substrates and corresponding enhancement factors. The regression coefficient $R^2 = 0.1242$. This could be readily concluded inspecting Fig. D.3 depicting Raman enhancement factor *vs*. $\Delta f(\alpha)$.

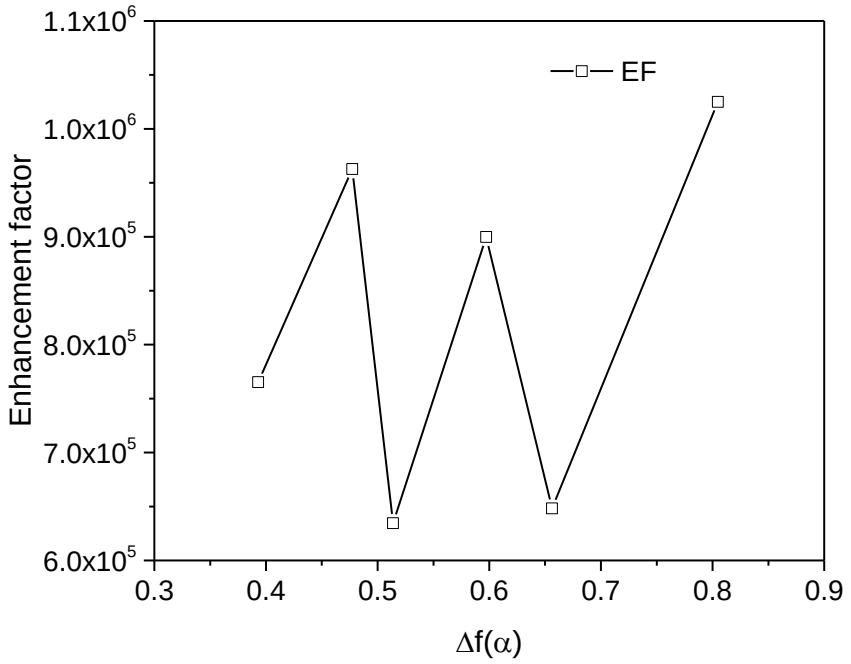

Fig. D. 3 The enhancement factor *vs.* degree of multifractality of the investigated substrates

Furthermore, multifractal sets can also be characterized on the basis of the generalized dimensions *Dq*, of the *q*th moment orders distribution, defined as [D.3, D.4]:

$$D_q = \frac{1}{q-1} \lim_{L \to 0} \frac{\log[\mu(q,L)]}{\log[L]} \quad \text{(D. 6)}$$

where μ(*q*, *L*) is the partition function that scles as

$$\mu(q, L) \sim L^{\tau(q)} \quad \text{(D. 7)}$$

Here τ(q) is the mass or correlation exponent of the qth moment order *q*.

Thus, the parameter *q* is a kind of a resolution parameter that enhances the regions corresponding to higher μ_ε values for positive values of *q*, and the regions of lower μ_ε values for negative values of *q*. Regarding the relation between multifractality and moment order *q* the curve f(α) is convex

with a single inflection point at the maximum with $q = 0$;) for $q = \pm\infty$, the slope is infinite and $\alpha_{min} = D_{+\infty}$, $\alpha_{max} = D_{-\infty}$. More rigorous discussion can be find in the literature [D.4]

The illustrative plots of D_q *vs*. q for samples 500^0C and 560^0C exhibiting different degrees of multifractality (0.80 and 0.65, respectively) are shown in Fig. D.4 below.

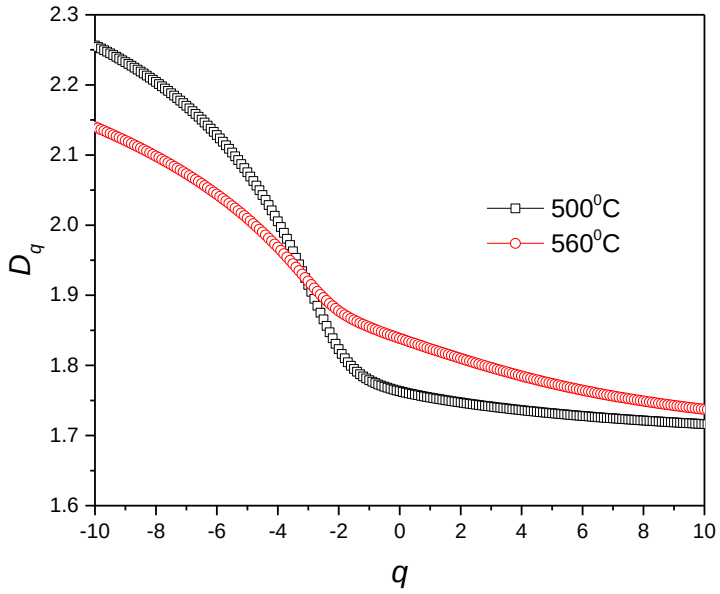

Fig. D.4 Generalized dimension *Dq vs. q* for structures with different degrees of multifractality. The sigmoidal curve corresponds to a structure with higher degree of multifractality and a more flat curve to a structure with lesser multifractality

Without going into the details plot of *Dq* vs. q is more or less a flat curve for monofractals and sigmoidal around $q = 0$ for multifractal structure, while a linear relationship between $\tau(q)$ and q implies a single fractal system characterized by one scaling exponent (homogeneous fractal).

On the other hand, variable slopes in a $\tau(q)$ *vs*. q relationship are indicative of a multifractal (heterogeneous) system [D.5]). A special case of the latter systems is the bifractal distribution, defined by two slopes dominating a $\tau(q)$ *vs.q* plot and related to different fractal dimensions. This is the case with our samples as clearly seen from representative plot of $\tau(q)$ *vs*. q (Fig. D.5). Here, the two ranges of $\tau(q)$ with different slopes corresponding to two different fractal dimensions can be easily identified. The crossover occurs at length scales of about 200 nm. Additional insight

into the scale at which crossover occurs could be provided by analysis of the auto-correlation length, since the autocorrelation function describes how well an image correlates with itself under conditions where the image is displaced with respect to itself in all possible directions [D.5, 6].

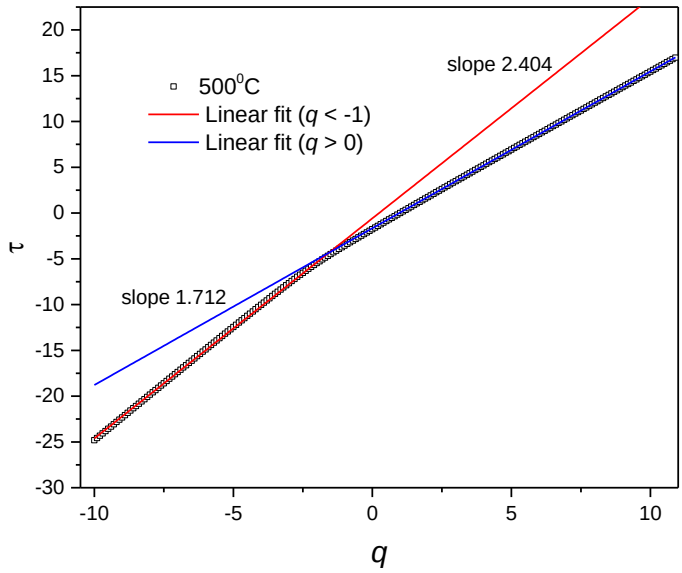

Fig. D.5 τ(q) *vs.* q for sample 500^{0}C (Δf (α) = 0.8). Two different slopes of the plot in regions q < 0 and q > 0 are related to two different fractal dimensions. The crossover occurs approximately at about 200nm.

References:

[D.1] Chhabra, A.B., and R.V. Jensen Direct determination of the f(α) singularity spectrum. Phys. Rev. Lett. 62 (1989) 1327–1330. https://doi.org/10.1103/PhysRevLett.62.1327

[D.2] Chhabra, A.B., C. Meneveu, R.V. Jensen, and K.R. Sreenivasan, Direct determination of the f (α) singularity spectrum and its application to fully developed turbulence. Phys. Rev. A 40 (1989) 18. U.S. Gov. Print Office, Washington, DC. 5284–5294. https://doi.org/10.1103/PhysRevA.40.5284

[D.3] Hentschel, H.G.E., and I. Procaccia, The infinite number of generalized dimensions of fractals and strange attractors. Physica D 8(1983) 435–444. https://doi.org/10.1016/0167-2789(83)90235-X

[D.4] JM. Barbaroux, F.Germinet and S. Tcheremchantsev, Generalized fractal dimensions: equivalences and basic properties, J. Math. Pures Appl. 80, 10 (2001) 977–1012 https://doi.org/10.1016/S0021-7824(01)01219-3

[D.5] Machs, J., F. Mas, and F. Sagues, Two representations in multi fractal analysis. J. Phys. A: Math. Gen. 28 (1995) 5607–5622. https://doi.org/10.1088/0305-4470/28/19/015

[D.6] R.P. Heilbronner, The autocorrelation function: an image processing tool for fabric analysis, Tectonophysics 212 (1992) 351–370,

https://doi.org/10.1016/0040-1951(92)90300-U

[D.7] Marteau, J., and M. Bigerelle. "Relation between surface hardening and roughness induced by ultrasonic shot peening." *Tribology International* 83 (2015): 105-113. https://doi.org/10.1016/j.triboint.2014.11.006

Declaration of Competing Interest

The authors declare that they have no known competing financial interests or personal relationships that could have appeared to influence the work reported in this paper.

CRediT author statement

D.R.: Conceptualization, Methodology, Formal analysis, Visualization, Writing- Original Draft, Reviewing and Editing,

H.G.: Investigation, Methodology, Resources, Validation, Writing - Review & Editing

M.I.: Supervision, Resources, Writing - Review & Editing, Funding acquisition